CORPORATE RESEARCH AND DEVELOPMENT • SCHENECTADY, NEW YORK

SILICON PHOTOVOLTAIC CELLS

by

R.N. Hall
Signal Electronics Laboratory

Report No. 80CRD274 January 1981

TECHNICAL INFORMATION SERIES

CLASS 1

GENERAL ELECTRIC

General Electric Company
Corporate Research and Development
Schenectady, New York

TECHNICAL INFORMATION SERIES

AUTHOR	SUBJECT	NO. 80CRD274
Hall, RN	solar cells	DATE January 1981
TITLE Silicon Photovoltaic Cells		GE CLASS 1
		NO. PAGES 24
ORIGINATING COMPONENT	Signal Electronics Laboratory	CORPORATE RESEARCH AND DEVELOPMENT SCHENECTADY, N.Y.

SUMMARY

The principles governing the performance of silicon solar cells are reviewed with emphasis on clarifying the essential concepts. Principal attention is devoted to the planar p-n junction cell and recent developments that have contributed to increased efficiency. Other solar cell structures are also reviewed and their relative advantages and shortcomings are discussed. Important areas where our present understanding is inadequate are pointed out and some common misconceptions are corrected.

KEY WORDS

solar cells, photovoltaics, silicon

INFORMATION PREPARED FOR ______________________

Additional Hard or Microfiche Copies Available From

Technical Information Exchange
Bldg. 81 Room A133, Schenectady, N.Y., 12345

RD-54 (1/80)

CONTENTS

Section		Page
	NOMENCLATURE	iv
1	INTRODUCTION	1
	1.1 Cells with Collecting Junctions at the Front Surface	1
	1.2 P^+-I-N^+ Cells	1
	1.3 Edge-Illuminated Multijunction Cells	2
2	SEMICONDUCTOR PROPERTIES OF SILICON	2
	2.1 Energy Gap, E_g	2
	2.2 Modification Caused by Large Impurity Concentrations — Heavy Doping Effects	2
	2.3 Intrinsic Carrier Concentrations, n_i	3
	2.4 Optical Absorption, α	3
	2.5 Mobilities and Diffusion Coefficients	3
	2.6 Lifetime, τ	4
	2.7 Diffusion Length, L_e and L_h	5
3	THE ELECTRICAL CHARACTERISTICS OF SOLAR CELLS	5
	3.1 The Curve Factor, f	6
	3.2 AM1 Short-Circuit Current Density	6
	3.3 Superposition	7
4	FRONT SURFACE JUNCTION CELLS, N^+-P-Ohmic AND N^+-P-P^+ CONFIGURATION	7
	4.1 Equivalent Circuit	8
	4.2 The J_{01} Component of the Dark Saturation Current; Emitter Efficiency	9
	4.3 The High-Low Emitter	10
	4.4 The J_{0n} Component of the Dark Saturation Current	10
	4.5 Series Resistivity, R_s	10
	4.6 Shunt Conductance, G_{sh}	12
	4.7 Reduced Curve Factor Due to R_s and G_{sh}	12
	4.8 Short-Circuit Current Density, J_{sc}	13
	4.9 Open-Circuit Voltage, V_{oc}	13
	4.10 Efficiency, η	15
	4.11 Temperature Dependence	15
5	OTHER CELLS WITH FRONT SURFACE COLLECTING JUNCTION	17
	5.1 MIS and SIS Cells	17
	5.2 Oxide Charge-Induced Inversion Layer Cells	18
	5.3 Double-Sided Junction Cells	18
6	P^+-I-N^+ CELLS	18
7	EDGE-ILLUMINATED MULTIJUNCTION CELLS	19
8	CONCLUDING REMARKS	21
	BIBLIOGRAPHY	21
	REFERENCES	21

NOMENCLATURE

Symbol	Definition
A	Junction area, cm^2
B	Coefficient for radiative recombination, cm^3/s
C	Optical concentration ratio
C_N, C_P	Auger recombination coefficients in n- and p-type silicon, cm^6/s
d	Spacing between grid lines, cm
D_e, D_h	Electron and hole diffusion coefficients, cm^2/s
E_F	Fermi energy, eV
E_g	Energy gap, eV
E_{g0}	Activation energy for n_i, eV
f	Curve factor
g	Dimensionless shunt conductance
G_{sh}	Shunt conductance, mho/cm^2
h	Coefficient describing injection into end regions, cm^4/s
j	Dimensionless current density
J	Current density, A/cm^2
ℓ	Length of grid lines, cm
L_e, L_h	Electron and hole diffusion lengths, cm
n	Electron concentration, cm^{-3}; also used as the diode quality factor (dimensionless), as in Equation 16.
n_i	Intrinsic carrier concentration, cm^{-3}
$n_{i,eff}$	Modification of n_i due to heavy doping, cm^{-3}
N_A	Acceptor dopant concentration, cm^{-3}
p	Hole concentration, cm^{-3}
P	Acceptor dopant concentration, cm^{-3}
r	Dimensionless series resistance parameter
R	Recombination rate, $cm^{-3}s^{-1}$
R_e	Resistivity due to emitter spreading resistance, ohm-cm^2
R_g	Resistivity due to resistance along grid lines, ohm-cm^2
R_s	Series resistivity, ohm-cm^2
$\mathcal{R}_e$	Series resistance due to emitter, ohms
S	Surface recombination velocity, cm/s
U	Dimensionless open-circuit voltage parameter
v	Dimensionless voltage parameter
w	Width of grid lines, cm
W	Thickness of base region, cm
x_j	Junction depth, cm

Greek Symbols

Symbol	Definition
α	Optical absorption coefficient, cm^{-1}
β	Temperature coefficient of efficiency, deg^{-1}
η	Solar cell efficiency, %
μ	Mobility, cm^2/volt-s
ϱ_e	Sheet resistance of emitter region, ohms/square
ϱ_m	Sheet resistance of grid metal, ohms/square
τ	Minority carrier lifetime, s

SILICON PHOTOVOLTAIC CELLS

R.N. Hall

1. INTRODUCTION

Developments in silicon solar cell technology have been taking place at an accelerated pace in recent years, stimulated by the awareness among the technical community of the need for a nonpolluting renewable source of electrical energy, by increased federal support, and by the possible emergence of a viable large-scale photovoltaic industry. The semiconductor principles which determine cell performance have been extended, new solar cell structures have emerged, and the analysis and understanding of their electrical characteristics have advanced on many fronts.

This report reviews the current status of work in this field. The current-voltage characteristic of the illuminated solar cell is discussed with emphasis on clarifying the essential concepts. Several important areas where our present understanding is inadequate are also pointed out and some common misconceptions are discussed. Silicon photovoltaic cells are made in many configurations, including the familiar p-n junction cell with its front-surface grid, metal-insulator (MIS) cells, interdigitated back contact (IBC) cells, and various forms of vertical multijunction (VMJ) cells. Principal attention is devoted to the planar p-n junction cell since it has achieved the greatest maturity both in theory and in application. It serves as a useful reference for comparison with other kinds of solar cell.

The emphasis in this report is upon measures which can be used to achieve the maximum cell efficiency. These are not always applicable to terrestrial power generation where cost considerations often require compromises in the quality of the initial silicon and in the fabrication methods that can be employed. Several important topics were found to be too complex to be dealt with in this report. These include discussions of the different crystal growth methods, cell fabrication practices and the consequences of using polycrystalline material, and the economics of the various approaches to cell manufacture.

It is hoped that this review will prove helpful to those working with cells made from other semiconductors as well as silicon. Silicon cell technology clearly illustrates the principles and constraints which determine cell performance, and this insight may suggest new avenues for achieving improved performance in cells made from other materials.

More than a dozen different types of silicon solar cells have emerged during recent years. For purposes of discussion, it will be convenient to group them into three different modes of operation.

1.1 Cells with Collecting Junctions at the Front Surface

The most common form of solar cell has a thin collecting junction at its front surface. This junction may be a diffused or ion implanted p-n junction, a metal-semiconductor Schottky barrier, or a metal-insulator-semiconductor (MIS) structure. The absorbed light produces minority carriers which diffuse to the junction and fall through the built-in field, producing a photocurrent. If this current is not drained off by a load, the junction develops an open-circuit voltage or "floating potential" due to the excess minority carrier population maintained within the semiconductor by the incident light. The back surface of the cell is often heavily doped (as in the back-surface field or BSF cell) to produce another built-in field region that reflects minority carriers back toward the collecting junction. In these cells the principal function of the BSF is to increase current collection by eliminating surface recombination at the back of the cell. Although conceptually one-dimensional structures, these cells involved a lateral flow of current in the thin front-surface layer which significantly affects their performance.

1.2 P^+-I-N^+ Cells

In these cells most of the light absorption takes place in silicon that is sufficiently pure, or the light is sufficiently intense, that the concentration of photo-generated carriers (electrons and holes) exceeds the background doping level in the I-region. This I-region is not actually intrinsic, but is usually made from 10 to 100 ohm-cm silicon which contains few enough majority carriers that the electrical performance can be modeled after the classical P^+-I-N^+ rectifier (Herlet, 1968; Berz, 1977). Under illumination, electrons and holes diffuse to the N^+ and P^+ electrodes where they are captured, generating a photocurrent. The cell may have the same configuration as the front surface cells described above, in which case the function of the rear junction is to generate an additional voltage by capture of one type of carrier while it reflects carriers of the opposite type. Alternatively, it may have both collecting junctions on the back, eliminating grid shadowing and losses due to recombination and spreading resistance in the front-surface layer. Conductivity modulation plays an essential role in reducing resistive losses in the substrate of P^+-I-N^+ cells and places a premium on achieving a long recombination lifetime in this region.

Manuscript received November 5, 1980

1.3 Edge-Illuminated Multijunction Cells

The cells of this class contain arrays of junctions that are oriented more or less edge-on to the incident light. This permits most of the light to enter the cell and be absorbed in the substrate region without having to pass through a heavily doped junction layer. Many different forms of multijunction cell have emerged, some featuring series interconnection or metallization patterns designed for operation in concentrator systems where the fabrication steps needed to achieve their more complex structures can be justified by their improved performance under high optical intensity.

2. SEMICONDUCTOR PROPERTIES OF SILICON

The discussion of silicon solar cells which follows involves a number of material parameters as described in several reviews (Baliga, 1980; Wolf, 1971; Sze, 1969). Those properties most instrumental in determining the design and analysis of cell performance are discussed below.

2.1 Energy Gap, E_g

The energy gap of pure silicon is accurately known (Barber, 1967; Varshni, 1967; Bludau et al., 1974). At room temperature, 300 K, its value is 1.120 eV, slightly below the optimum for solar energy conversion. In the range near and somewhat above room temperature, where solar cells are usually operated, the energy gap decreases linearly with temperature as described by,

$$E_g(T) = 1.120 - 2.8 \times 10^{-4}(T - 300\text{ K})\text{ eV} \quad (1)$$

2.2 Modifications Caused by Large Impurity Concentrations — Heavy Doping Effects

Most cells contain one or more heavily doped regions where the normal properties of the semiconductor are modified by "heavy doping effects." In an n-type semiconductor, for example, the high concentration of donor impurities causes the states near the conduction band edge to become smeared out and merge with the donor levels. Also, at sufficiently high donor concentrations the Fermi level moves up into the conduction band and the semiconductor becomes degenerate. This happens for donor concentrations greater than 2.35×10^{19} cm^{-3} at room temperature, assuming that the conduction band density of states is not changed at these high doping levels. In p-type silicon, degeneracy is achieved for acceptor concentrations greater than 1.34×10^{19} cm^{-3}. In this range the transport properties of the majority carriers are largely determined by those electrons near the Fermi surface away from the smeared-out band edge. The semiconductor resembles a metallic conductor, with the electron distribution governed by Fermi rather than Boltzmann statistics.

On the other hand, any minority carriers (holes) that may be present occupy states near the valence band edge. This band is also modified by the donor impurities, so the holes move in the tail states of the valence band and can be expected to have transport properties somewhat different from their behavior as majority carriers at a comparable doping level.

Heavy doping effects are important because they are involved in the principal compromises that must be made in solar cell design. In cells with front-surface junctions, this region must be thin enough that carriers generated near the surface can reach the junction and be collected. On the other hand, it must have a low sheet resistance to minimize spreading resistance losses and therefore must be heavily doped. Another compromise results because the open-circuit voltage developed by a cell tends to increase as the impurity concentration on both sides of the junction is increased. This reaches a limit, however, due to several heavy doping effects which combine in ways that are not yet clearly understood, and thereafter the output diminishes.

A proper description of minority carrier injection in heavily doped material is presently lacking, but several important considerations are evident. First of all, Fermi statistics must be used to describe the majority carrier distribution in degenerate material. Secondly, the presence of the doping impurities causes the semiconductor to behave as though its energy gap had been decreased by an amount, ΔE_g, as indicated in Figure 1. The band gap shrinkage as a function of doping concentration has been inferred from optical absorption data and from measurements of diode and transistor characteristics. The optical evidence comes from transitions between states that

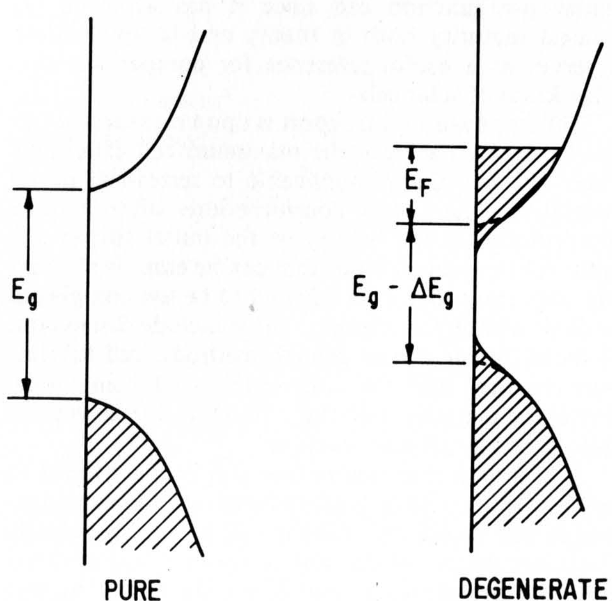

Figure 1. Modification of the density-of-states diagram of a semiconductor caused by a large (degenerate) donor concentration. The bands are considered to shift rigidly toward each other by an amount ΔE_g, while the Fermi level moves an amount E_F into the conduction band. Band edge tailing is also indicated.

are well away from the band edges, so they reflect the "rigid shift" indicated by the diagram. On the other hand, the electrical measurements sense the energy difference between the Fermi level of the majority carriers and those tail states of the opposite band where the minority carriers can be regarded as mobile. This corresponds to a "mobility band edge" (Redfield, 1975). Electrical measurements therefore yield somewhat greater values for the effective band gap shrinkage. However, it must be emphasized that the magnitude of ΔE_g and its dependence upon dopant species and concentration have not yet been established conclusively and are subjects of considerable current interest and discussion (Mahan, 1980; Redfield, 1980; Fossum et al., 1979; Possin et al., 1980; Keyes, 1976). Thirdly, the minority carriers can be expected to exhibit a reduced mobility due to tailing caused by the majority doping impurties. The behavior of heavily doped silicon is further complicated by the extremely short minority carrier lifetime, due principally to Auger recombination. Heavy doping effects and their implications for device performance have been discussed in several recent publications (Abram et al., 1978; Lauwers et al., 1978; Marshak and Shrivastava, 1979; de Graaff et al., 1977; Fistul', 1969; Hauser and Dunbar, 1977; Heasell, 1980; Tang, 1980).

2.3 Intrinsic Carrier Concentration, n_i

The intrinsic carrier concentration is instrumental in determining the dark saturation current and hence the open-circuit voltage of a solar cell. Its variation with absolute temperature T is given by (Barber, 1967),

$$n_i = 3.87 \times 10^{16} T^{3/2} \exp(-E_{g0}/2kT) \quad (2)$$

where $E_{g0} = 1.210$ eV. At room temperature (300 K) this expression gives $n_i = 1.35 \times 10^{10}$ cm^{-3}. It increases by a factor of 2.23 in the next 10 °C.

The effects of band gap shrinkage and degeneracy discussed in the previous paragraph result in an increased equilibrium pn product in heavily doped material (Abram et al., 1978; Slotboom, 1977) given by,

$$n_{i,eff}^2 = n_i^2 \exp(\Delta E_g/kT) \{F_{1/2}(E_F/kT) \exp(E_F/kT)\} \quad (3)$$

where $F_{1/2}$ is the Fermi integral and E_F is the amount by which the Fermi level has moved into the conduction band. The first exponential factor, which is always greater than unity, represents the effects of band-gap shrinkage. The bracketed factor accounts for degeneracy; its reciprocal is the activity coefficient (Landsberg, 1980). It is always less than unity so these factors tend to offset each other. While the use of $n_{i,eff}$ makes it possible to use Boltzmann statistics beyond its range of applicability, it should be done with caution since it may also obscure some important aspects of junction behavior.

2.4 Optical Absorption, α

The minority carrier generation rate within an illuminated solar cell is determined by the spectral distribution and coefficient for band-to-band optical absorption. The dependence of the absorption coefficient of silicon upon temperature and photon energy has been reviewed recently for application to solar cell analysis (Weakliem and Redfield, 1979). Since silicon is an indirect transition semiconductor its absorption coefficient increases slowly with energy above the absorption edge and consequently a rather thick layer is required to absorb most of the incident radiation. For example, a thickness of 200 microns is required for 95% absorption of the AM1 spectrum. For this reason, silicon cells are generally made thick enough to be self-supporting. Thin-film cells, on the other hand, must be made from semi-conductors having very strong optical absorption and they require a supporting substrate whose properties must be taken into account as an integral part of the cell structure.

2.5 Mobilities and Diffusion Coefficients

The electron and hole mobilities in pure silicon are given by,

$$\mu_e = 1360\,(T/300)^{-2.42}\ \text{cm}^2/\text{V}-\text{s} \quad (4a)$$

and

$$\mu_h = 495\,(T/300)^{-2.20}\ \text{cm}^2/\text{V}-\text{s}. \quad (4b)$$

In doped silicon, these parameters are decreased by impurity scattering, falling roughly a factor of 10 as the impurity concentration is increased from 10^{16} to 10^{19} cm^{-3}. At still higher donor or acceptor concentrations, the semiconductor behaves "metallic" and the mobilities assume nearly constant values, $\mu_e \sim 90$ cm^2/V – s and $\mu_h \sim 48$ cm^2/V – s. Curves showing the variation of μ_e and μ_h with temperature and impurity concentration have been published recently (Li and Thurber, 1977; Li, 1978).

The output of a solar cell is derived from the diffusive flow of minority carriers to some form of collecting junction so the diffusion coefficient D is of more direct concern than the mobility. They are connected by the Einstein relation, $D = kT\mu/q$, so in pure silicon at room temperature

$$D_e = 35.1\,(T/300)^{-1.42}\ \text{cm}^2/\text{s} \quad (5a)$$

and

$$D_h = 12.7\,(T/300)^{-1.20}\ \text{cm}^2/\text{s}. \quad (5b)$$

In degenerate material the diffusion coefficients for majority carriers decrease to approximately 2 and 1 cm^2/s, respectively. Minority carriers presumably diffuse somewhat more slowly, reflecting the properties of the modified "tail states."

2.6 Lifetime, τ

The minority carrier lifetime is limited by several recombination mechanisms. The dominant process in most silicon is Hall-Shockley-Read recombination which proceeds via defects having energy levels deep within the energy gap. In the simplest case where the only recombination center present is one that produces a single level in the energy gap, the recombination rate is given by,

$$R_{\text{HSR}} = \frac{np - n_i^2}{\tau_{po}(n+n_r) + \tau_{no}(p+p_r)} \tag{6}$$

and the lifetime at low injection level is

$$\tau_{\text{HSR}} = \frac{\tau_{po}(n+n_i) + \tau_{no}(p+p_r)}{n+p} \tag{7}$$

The parameters n_r and p_r describe the location of the level within the energy gap; they are the electron and hole concentrations which would prevail if the sample were doped so that its Fermi level coincided with the recombination center. Thus the position of the level above midgap is given by $\Delta E_r = (kT/q)\ln(n_r/n_i) = (kT/q)\ln(n_i/p_r)$. In strongly doped silicon such that $n \gg n_r$ or $p \gg p_r$ the lifetime assumes a constant value, τ_{po} or τ_{no}, respectively, independent of the doping level. These "plateau lifetimes" have the form $\tau_{po} = 1/(N_r\sigma_r v)$ where N_r is the concentration per unit volume of centers, σ_r is their capture cross section, and v is the thermal velocity of the electrons or holes.

Actual samples of silicon can be expected to have several sets of recombination centers present. In most junction devices the principal concern is usually with the generation current that is produced within the space-charge layer of a reverse biased junction where $n = p = 0$. This is dominated by those defects having energy levels closest to midgap (Sah et al., 1957). Solar cells, on the other hand, are operated under forward bias with both types of carrier present so according to Equation 6 the criterion that determines whether a defect will be effective as a recombination center (for the same concentration and cross section) is that its energy level must be closer to mid-gap than the quasi Fermi Level of the sample. In other words, all defects having $(n_r + p_r)$ less than the majority carrier concentration are effective in limiting the lifetime, so there is a tendency for the apparent values of τ_{po} and τ_{no} as determined from experiment to decrease instead of remaining constant as the doping level is increased, as has been noted by Kendall, 1969. The lifetime due to deep-level recombination depends upon the quality of the starting material and upon many details of the cell fabrication process. Changes in minority carrier lifetime during fabrication have been reported by Graff and Fischer, 1979. With reasonable care HSR lifetimes as high as 20 to 50 μs can be achieved in the base regions of finished cells.

Under conditions of high-level operation, where the minority carrier concentration becomes equal to or greater than n_r, p_r, and the equilibrium concentration of majority carriers, τ_{HSR} changes to a new value which is called the high-level lifetime, τ_∞.

$$\tau_\infty = \tau_{po} + \tau_{no} \tag{8}$$

According to the HSR model, τ_∞ can be either smaller or larger than the low-level lifetime. The rather pure ($\sim$100 ohm-cm) n-type silicon used in power devices generally exhibits a modest decrease in lifetime at high injection levels (Schuster, 1965). On the other hand, the behavior of solar cells under strong illumination sometimes indicates an increased high-level lifetime (Meulenberg et al., 1980).

Auger recombination becomes the dominant process in strongly doped n- or p-type silicon (Dziewior and Schmid, 1977; Svantesson and Nilsson, 1979). The net recombination rate is given by,

$$R_{\text{Auger}} = (C_N n + C_P p)(np - n_i^2) \tag{9}$$

In extrinsic material the Auger lifetime decreases rapidly as the majority carrier concentration increases. In n-type silicon it is given by

$$\tau_{A,N} = 1/C_N n^2 \tag{10a}$$

where $C_N = 2.8 \times 10^{-31}$ cm^6 s^{-1}. In p-type silicon, it varies as

$$\tau_{A,P} = 1/C_P p^2 \tag{10b}$$

where $C_P = 1 \times 10^{-31}$ cm^6 s^{-1}. The coefficients C_N and C_P are nearly independent of temperature, increasing less than 30% between 77 K and room temperature (Dziewior and Schmid, 1977). The theoretical and experimental evidence indicate that these equations remain valid in degenerately doped material (Lochmann, 1978). While these Auger coefficients are commonly regarded as intrinsic properties of silicon, there are other experiments which indicate much lower values (Van Meerbergen et al., 1978; Possin et al., 1980; Weaver and Nasby, 1980). The possibility should be kept in mind that the values for C_N and C_P given above may have been based on transitions involving defects and that the true Auger coefficients are significantly smaller than has generally been believed.

Radiative recombination also occurs in silicon, but it is too weak to have any significant effect upon the minority carrier lifetime. The recombination rate for this process is given by $R_{\text{rad}} = B(np - n_i^2)$, where $B = 0.95 \times 10^{-14}$ cm^3/s (Schlangenotto et al., 1974). The corresponding lifetime expression is $\tau_{\text{rad}} = 1/B(n+p)$.

The lifetime due to all of these processes is determined by their reciprocal sum,

$$\frac{1}{\tau} = \frac{1}{\tau_{\text{HSR}}} + \frac{1}{\tau_{\text{Auger}}} + \frac{1}{\tau_{\text{rad}}} \tag{11}$$

2.7 Diffusion Length, L_e and L_h

The current generated by a solar cell is largely determined by the diffusive flow of minority carriers to collecting junctions. The distance such a carrier can travel is described by the diffusion length, $L = \sqrt{D\tau}$. Figure 2 indicates the variation of diffusion length with majority carrier concentration for n- and p-type silicon. Both D and τ decrease as the doping level is increased, as discussed above. The curves of Figure 2 were calculated using the Auger coefficients of Equation 10 and two choices of τ_{HSR}, 10 and 50 μs. The latter is representative of a cell made from good quality silicon with careful processing. Shorter HSR lifetimes, 10 μs or less, may result from inferior starting material or recombination centers introduced during cell fabrication.

Two regions of Figure 2 are of particular interest. The substrate, or base region, typically has a thickness of 100 to 200 microns and a doping level in the range 10^{15} to 10^{17} cm^{-3}. Efficient current collection from the base region requires a diffusion length that is greater than the cell thickness. When high quality single-crystal (electronic grade) silicon can be used this condition is not difficult to fulfill, although it becomes more of a problem at high substrate doping levels. On the other hand, it is one of the principal criteria that must be met by the "solar grade" silicon being developed to meet the cost constraints of terrestrial photovoltaic power generation. This material must be sufficiently free of deep-level impurities to yield an adequate diffusion length.

The second regime corresponds to the "emitter region" of a cell having a diffused front-surface junction. These regions are typically made one or two tenths of a micron thick with doping concentrations in the range 1 to 5 $\times$ 10^{20} cm^{-3} where the lifetime becomes very short due to Auger recombination. The corresponding diffusion length indicated by Figure 2 is a few tenths of a micron or less. Since this is comparable to the thickness of the emitter region there would appear to be a high probability that a carrier generated anywhere in the emitter region would be able to diffuse to the junction and be collected. Such a region is often called a "transparent emitter" (Shibib et al., 1979).

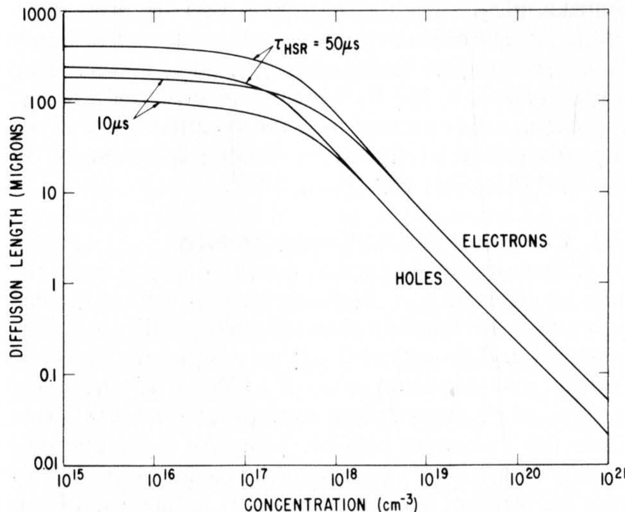

Figure 2. Minority carrier diffusion length vs majority carrier concentration, assuming HSR and Auger recombination.

This conclusion must be modified by two considerations. Firstly, if the front surface of the cell has a high surface recombination velocity it will be a sink for minority carriers and fewer of them will survive and be able to diffuse to the junction. For this reason it has been found to be advantageous to grow a thin layer of oxide over the front of the cell before adding the anti-reflection coating (Fossum et al., 1979). Secondly, in actual solar cells the emitter regions are made with strong concentration gradients which produce built-in electric fields (drift-fields) that can significantly change the effective diffusion length. In the absence of band-gap narrowing the drift-field would be in a direction to drive the minority carriers toward the junction and would be strong enough to make the effective diffusion length several times greater than that indicated by Figure 2. Band-gap narrowing tends to reduce the built-in field; in fact, the large ΔE_g's indicated by some of the electrical measurements call for a reversal of the built-in field, which would tend to drive the minority carriers toward the surface and reduce the collection efficiency.

3. THE ELECTRICAL CHARACTERISTICS OF SOLAR CELLS

A photovoltaic cell is a semiconductor diode with provision for admitting optical excitation to generate electron-hole pairs in the proximity of the junction. In the dark its behavior resembles the $J \sim \exp(qV/kT) - 1$ characteristic of an ideal p-n junction. When illuminated, an additional current component is added which shifts the characteristic along the current axis by an amount $-J_{sc}$, where J_{sc} is the short-circuit current density and is nearly independent of voltage. It is more convenient to take the opposite sign for the current flow so the current delivered to a passive load will be positive. The elemental form for the solar cell characteristic then becomes,

$$J = J_{sc} - J_{01}[\exp(qV/kT) - 1] \quad (12)$$

J_{01} is the "dark saturation current density" which results from the thermal generation of minority carriers within the semiconductor. It should be made as small as possible to maximize the output voltage generated by the cell. This is the characteristic for the case where the minority carrier concentration in the base is always small compared with the majority carrier concentration.

The behavior of this equation is illustrated by Figure 3. When a load is attached to the cell it delivers current at a voltage that depends upon the load impedance. If the load impedance is zero the cell generates

its short-circuit current J_{sc} which is proportional to the illumination intensity. If the load is disconnected it develops an open-circuit voltage given by

$$V_{oc} = \frac{kT}{q} \ln (J_{sc}/J_{01} + 1) \approx \frac{kT}{q} \ln (J_{sc}/J_{01}) \quad (13)$$

Since J_{sc}/J_{01} is typically of order 10^{10} to 10^{14} this approximation introduces negligible error.

Maximum power is delivered when the load impedance is properly matched giving

$$P_{max} = J_m V_m = f J_{sc} V_{oc} \quad (14)$$

The curve factor, f, depends upon the "sharpness" of the current-voltage characteristic. An "ideal" silicon cell having a characteristic described by Equation 12 and illuminated at approximately one sun intensity to give $V_{oc} = 0.6$ volt at 300 K would have $f = 0.827$. Real cells often achieve curve factors in the range 0.75 to 0.8 volt.

The equation corresponding to Equation 12 for the ideal P^+-I-N^+ cell is

$$J = J_{sc} - J_{02} [\exp (qV/2kT) - 1] \quad (15)$$

This form follows from the assumption that the current is due to HSR recombination in the base region under high-level conditions where the lifetime is described by Equation 8. The electron and hole concentrations in the base are equal and are determined by the cell voltage which is equally divided between the P^+I and IN^+ junctions, accounting for the factor of 1/2 in the exponential.

3.1 The Curve Factor, f

The current-voltage characteristic of a solar cell is often written in the general form

$$J = J_{sc} - J_{0n}[\exp (qV/nkT) - 1] \approx J_{sc} - J_{0n}\exp (qV/nkT) \quad (16)$$

The parameter, n, appearing in these equations determines the sharpness of the $J-V$ characteristic and hence the magnitude of the curve factor as can be seen from Figure 3. In all cases of practical interest $J_{0n} \ll J_{sc}$ so the second form of this equation is an excellent approximation. With this approximation we have $V_{oc} = (nkT/q) \ln(J_{sc}/J_{0n})$ so the cell characteristic can be written in the form

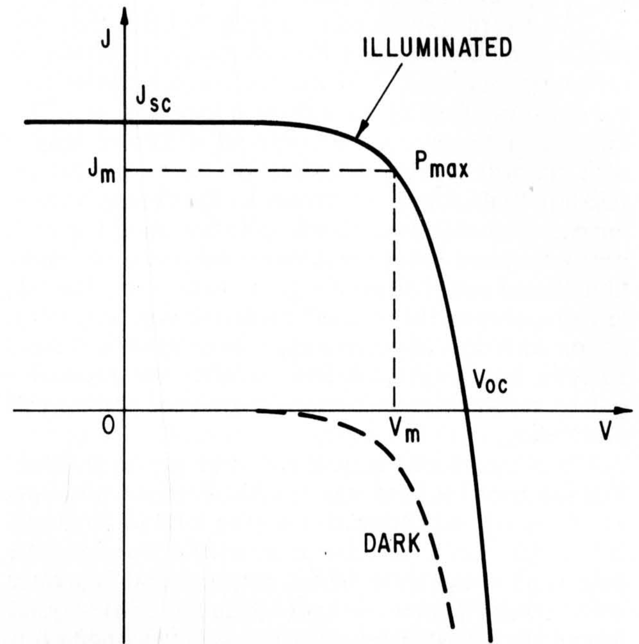

Figure 3. Dark and illuminated current-voltage characteristics of a solar cell. Maximum power is delivered at $P_{max} = J_m V_m = f J_{sc} V_{oc}$.

$$\frac{J}{J_{sc}} = 1 - \exp\left\{\frac{qV_{oc}}{nkT}\left[\frac{V}{V_{oc}} - 1\right]\right\}$$

or

$$j = 1 - \exp [U(v-1)] \quad (17)$$

where $j = J/J_{sc}$, $v = V/V_{oc}$, and $U = qV_{oc}/nkT$. The curve factor is equal to the maximum value of the (jv) product, which is seen to be a function of the single dimensionless variable, U. $f(U)$ and its derivative, df/dU, can be evaluated numerically with results shown in Figure 4. The lower scale gives V_{oc} for the case $n = 1$ and $T = 300$ K, which is of principal interest for silicon cells operated near room temperature. Further discussion of the curve factor can be found in Hovel, 1975, p 61; and Green, 1977.

3.2 AM1 Short-Circuit Current Density

The short-circuit current density depends upon the rate of generation of minority carriers within the cell and upon the fraction that are able to diffuse to the junction and be collected. If we assume the standard (but rather optimistic) value of 1 kW/m^2 for the power density of unconcentrated sunlight at the earth's surface, the maximum possible value for J_{sc} is approximately 45 mA/cm^2 corresponding to one electron hole pair per incident photon with energy greater than $E_g = 1.12$ eV. A range of values for this limiting photocurrent can be found in the literature but reliable

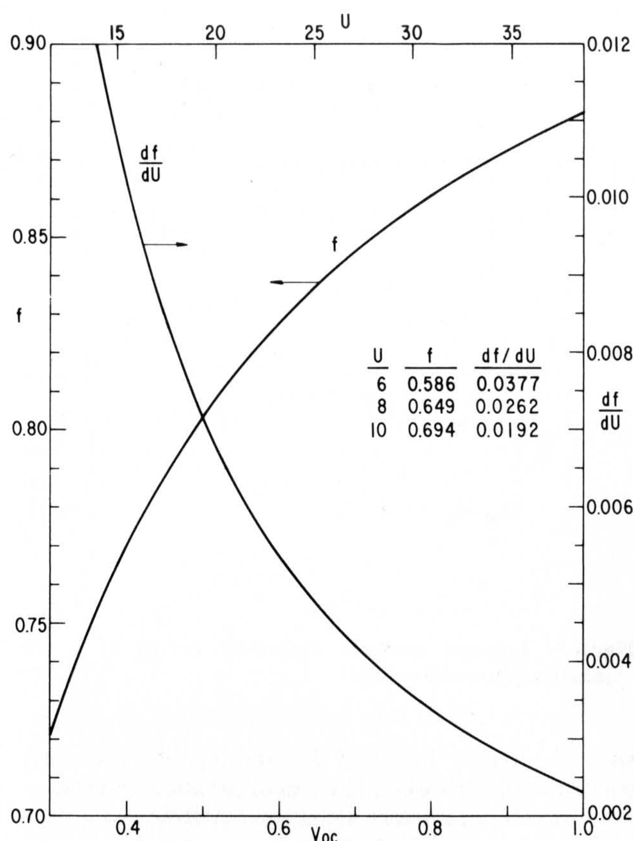

Figure 4. The curve factor f and its derivative with respect to voltage. The upper scale gives the dimensionless parameter, $U = qV_{oc}/nkT$. The lower scale shows V_{oc} for the case $n = 1$ and $T = 300$ K. The table (inset) gives additional values of f and df/dU.

documentation is difficult to obtain. The value 43 mA/cm^2 is obtained by correcting the AM1.5 spectrum (ERDA, 1977) which has a power density of 844 W/m^2 to 1 kW/m^2. The AM1 spectrum is somewhat richer in near band-edge radiation and would therefore give a slightly greater value for J_{sc}. A recent analysis by Sah gives 37.1 mA/cm^2 for 891 W/m^2 for AM1 insolation which corresponds to 41.6 mA/cm^2 at 1 kW/m^2 (Sah, 1978).

A more realistic value for the maximum achievable J_{sc} is obtained by considering only radiation that can be absorbed in ~200 microns of silicon which corresponds approximately to the spectrum beyond $h\nu$ = 1.24 eV. A calculation similar to that above gives 38 mA/cm^2 instead of 43 mA/cm^2 for the AM1.5 spectrum, or approximately 40 mA/cm^2 for 1 kW/m^2 of AM1 insolation. Wolf has obtained values as high as 41 to 42 mA/cm^2 in his calculations of the limit efficiency for specific cell geometries using the same insolation (Wolf, 1980).

Several factors can be expected to reduce J_{sc} below this value in actual cells. Front surface reflection losses can be reduced to only a few percent by applying an antireflection layer and by "texture etching" as described in Section 4. Shadowing by the front surface grid can be expected to cause an additional loss of 5 to 15% in typical cells. The current collected by the junction is reduced further by recombination of the photogenerated carriers in the bulk and at the surface and junction regions of the silicon.

The change of energy gap with temperature described by Equation 1 will tend to cause an increase in short-circuit current with temperature. This dependence can be calculated from the photon flux near the band edge relative to that in the entire absorbed spectrum giving,

$$\frac{1}{J_{sc}} \frac{dJ_{sc}}{dT} = 3 \times 10^{-4} \text{ per degree K} \qquad (18)$$

This variation is small compared with the changes of other solar cell parameters discussed later in Section 4.11.

3.3 Superposition

Equations 12 and 15 imply that illumination causes a simple translation of the current-voltage characteristic along the current axis. While this is a useful concept, it is not exact and its limitations should be kept in mind (Lindholm et al., 1979; Tarr and Pulfrey, 1980). The more common instances where superposition fails to apply are:

- Modifications of the *J-V* characteristic caused by series resistance cannot be described by a simple translation.
- Superposition also fails if the injection level in the base goes from low-level to high-level as the light intensity is increased.

4. FRONT SURFACE JUNCTION CELLS, N$^+$-P-Ohmic AND N$^+$-P-P$^+$ CONFIGURATION

The planar front surface junction cell will be discussed in some detail here since it is the form that has been most intensively developed. The analysis can be extended to other kinds of cells employing front surface collection with minor modification.

The construction of a silicon solar cell generally includes most of the features shown in Figure 5 which illustrates the N$^+$ front junction configuration. The photocurrent is collected by a shallow N$^+$ junction formed over the front surface. This layer must be thin enough to allow light to penetrate through it to the more lightly doped base. A metal grid is provided to make contact with the front layer without obstructing too much light and to minimize resistive losses due to the lateral flow of current in it. The loss of light by front surface reflection is minimized by applying a quarter-wave antireflection coating (Revesz et al., 1976; Iles, 1977; Kern and Tracy, 1980), and by "texture etching" the surface to produce a myriad of pyramids which trap the incident light by multiple reflection (Restrepo and Backus, 1976; Arndt et al., 1975).

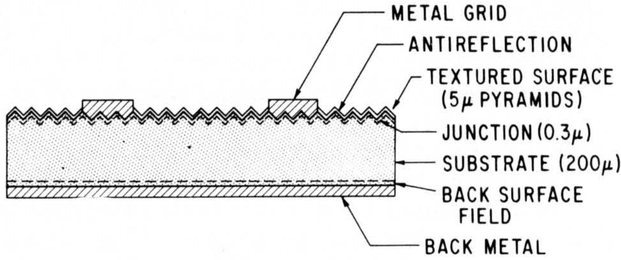

Figure 5. Silicon solar cell construction.

4.1 Equivalent Circuit

A real solar cell is more than a simple one-dimensional structure and it is not adequately represented by Equation 12. A more accurate description is obtained by taking into account the following additional features:

- Inclusion of a series resistance term to account for the difference between the terminal voltage and that which actually appears across the junction.
- A shunt conductance term to represent current leakage across the junction.
- Additional current components varying as $\exp(qV/nkT)$, where $n \approx 2$ or greater.

These can be represented by the equivalent circuit shown in Figure 6. This, of course, is not an exact representation since a real cell consists of a distributed network of cell elements connected across an R_s transmission line. Nevertheless, it gives sufficient accuracy for most purposes and is widely used as the basis for analyzing cell performance. This circuit gives the following *J-V* characteristic for the photovoltaic mode of operation:

$$J = J_L - J_{01}\left[e^{\frac{q}{kT}(V+JR_s)} - 1\right] - J_{0n}\left[e^{\frac{q}{nkT}(V+JR_s)} - 1\right] - G_{sh}(V+JR_s) \tag{19}$$

J_L is a constant current generator representing the photogenerated current. The appearance of J on the right of this equation when $R_s \neq 0$ accounts for superposition failure when the series resistance is significant.

The short-circuit current density will be somewhat less than J_L if G_{sh} is appreciable. Setting $V = 0$ we obtain

$$J_{sc} \approx \frac{J_L}{1 + G_{sh}R_s} \tag{20}$$

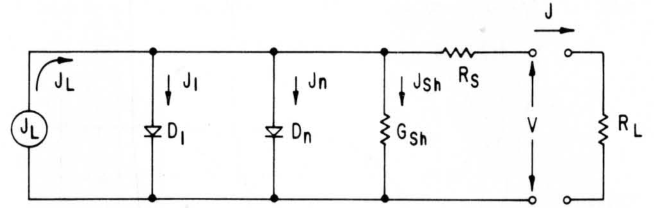

$$J_l = J_{0l}\left(e^{\frac{q}{kT}(V + JR_S)} - 1\right)$$

$$J_n = J_{0n}\left(e^{\frac{q}{nkT}(V + JR_S)} - 1\right)$$

$$J_{Sh} = G_{Sh}(V + JR_S)$$

$$J = J_L - J_l - J_n - J_{Sh}$$

Figure 6. Lumped constant equivalent circuit of a p-n junction photovoltaic cell.

since the terms involving J_{01} and J_{0n} are then very small compared with J_L in cases of practical interest.

The cell parameters are often determined by measuring the dark *J-V* characteristic, assuming that the same values apply when the cell is operated in the photovoltaic mode. The corresponding equation is obtained by setting $J_L = 0$ in Equation 19 and reversing the sign of J to make it positive. This gives for the dark current-voltage characteristic:

$$J = J_{01}\left[e^{\frac{q}{kT}(V-JR_s)} - 1\right] + J_{0n}\left[e^{\frac{q}{nkT}(V-JR_s)} - 1\right] + G_{sh}(V-JR_s) \tag{21}$$

The contributions of the different terms of this equation are illustrated in Figure 7 with parameter values chosen to represent the *J-V* characteristic of a typical silicon solar cell.

Comparing Equations 19 and 21, it will be seen that the dark current subtracts from the photocurrent that can be generated by a solar cell. It is the exponential increase of the dark current with voltage which limits the open-circuit voltage to a value which in silicon cells is approximatley 0.6 volt under one sun illumination. The cell parameters appearing in these equations should

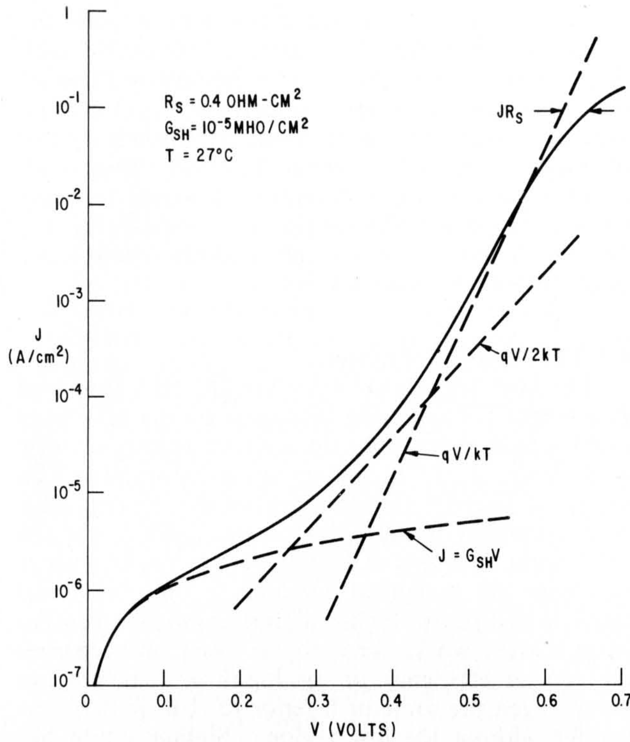

Figure 7. Dark current calculated from Equation 21 with $n = 2$. J_{01} and J_{02} were chosen to make $J_1 = 40$ mA/cm^2 and $J_2 = 2$ mA/cm^2 at $V = 0.6$ volt.

therefore be made as small as possible to minimize the dark current, as discussed in the following sections.

4.2 The J_{01} Component of the Dark Saturation Current; Emitter Efficiency

Our discussion of the factors which determine J_{01} will be directed to N$^+$-P-Ohmic and N$^+$-P$^+$-P$^+$ cells since analogous arguments apply to the opposite configuration. It is sufficient to consider one-dimensional structures as shown in Figure 8. We are concerned with the diffusion currents J_n and J_p which are injected into opposite sides of the junction when a forward bias is applied. Current components due to other mechanisms will be discussed later.

For a preliminary evaluation of J_{01} we note that the impurity concentration in the N$^+$ region is much greater than that of the base; consequently this junction can be expected to have a high emitter efficiency so we assume that J_{01} is due entirely to electrons injected from the N$^+$ region (often called the emitter) into the base. With this assumption J_{01} is easily evaluated. For the N$^+$-P-Ohmic cell the metal contact on the back serves as a perfect sink for electrons (surface recombination rate S = ∞ at this boundary), giving

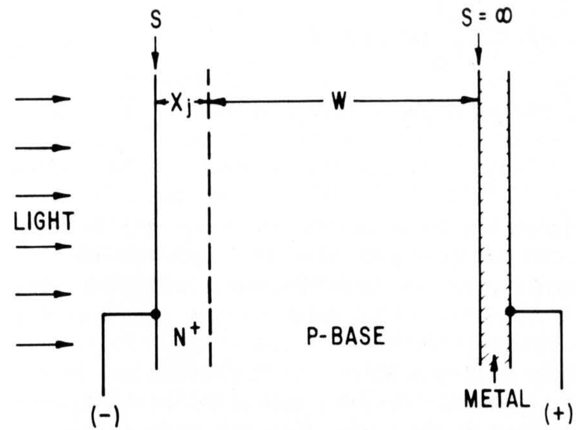

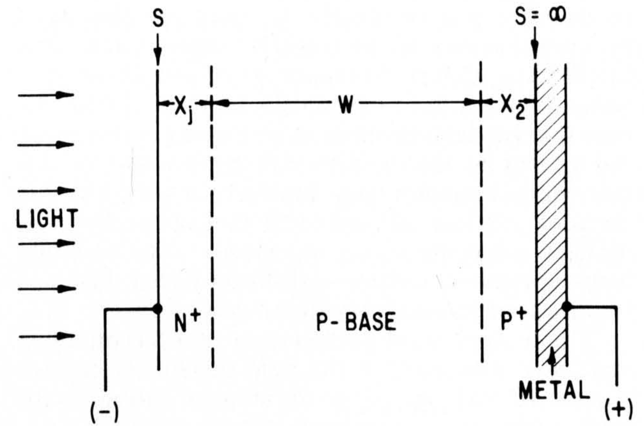

Figure 8. Basic N$^+$P cell configurations.

$$J_{01} = \frac{qD_e n_i^2}{N_A L_e} \coth\left(W/L_e\right) \qquad (22a)$$

$$\rightarrow qD_e n_i^2/N_A W \quad \text{if } L_e >> W \qquad (22b)$$

$$\rightarrow qD_e n_i^2/N_A L_e \quad \text{if } L_e << W \qquad (22c)$$

D_e and L_e are the electron diffusion coefficient and diffusion length in the base, and N_A is the acceptor concentration there.

The N$^+$-P-P$^+$ cell is called a back surface field (BSF) cell because the high-low junction at the back produces a built-in field which reflects minority carriers. Assuming complete reflection at the P-P$^+$ junction ($S = 0$) we obtain,

$$J_{01} = \frac{qD_e n_i^2}{N_A L_e} \tanh (W/L_e) \qquad (23a)$$

$$\rightarrow qn_i^2 W/N_A \tau \quad \text{if } L_e >> W \qquad (23b)$$

$$\rightarrow qD_e n_i^2/N_A L_e \quad \text{if } L_e << W \qquad (23c)$$

Comparing these results, we note that for any given cell thickness and diffusion length the BSF cell is always superior to the N^+-P-Ohmic cell. Both types of cell are improved by using material with a longer minority carrier lifetime.

These equations also indicate that J_{01} can be reduced, apparently without limit, by increasing the doping level in the base. Experimentally, however, it is found that this approach is no longer fruitful for $N_A > 10^{17}cm^{-3}$ (Hauser and Dunbar, 1977; Iles and Soclof, 1975; Fossum et al., 1978). As the doping level is increased further, the emitter efficiency begins to decrease and eventually J_{01} becomes dominated by the properties of the front N^+ region rather than by the base. Cell performance is further affected by a reduction in J_{sc} due to the shorter minority carrier lifetime that is encountered in more heavily doped material. Most of the experimental results indicate that there is an optimum base doping level somewhere in the range 10^{16} to $10^{17}cm^{-3}$ (0.3 to 2 ohm-cm) where the best cell performance is achieved. The optimum base doping level is somewhat higher in cells designed for operation in concentrated sunlight.

The analysis of cell performance near this optimum must take into account the hole current J_h injected into the N^+ layer as well as the electron current in the base, since both components contribute to J_{01}. J_h cannot be described by simple analytical equations like (22) and (23) for several reasons. The analysis is hindered by the lack of understanding of the heavy doping effects discussed in Section 2.2 and by the strong concentration gradient that generally exists in the N^+ region. Furthermore, this region is often made thin enough (0.1 to 0.2 micron) that surface recombination must be taken into account at the front surface of the cell and under the metal grid contacts in spite of the very short minority carrier lifetime (Shibib et al., 1979; Fossum et al., 1979). Under these circumstances it is important to minimize the area of contact between the grid and the N^+ region to suppress recombination at that interface (Lindmayer and Allison, 1976).

The best insight is often obtained by numerical device modeling which provides a means for taking these effects into account and evaluating their importance (Fossum, 1976; Weaver and Nasby, 1980; Dunbar and Hauser, 1977; Lauwers et al., 1978). Further elucidation of the factors which determine minority carrier injection into heavily doped emitters is provided by a recent analytical treatment (Amantea, 1980).

An alternative approach which may provide the basis for an analytical description of the emitter efficiency in solar cells is the use of the "h coefficients" that have been developed to describe injection into the end regions of transistors and PIN power devices (Burtscher et al., 1975; Berz et al., 1979). These were initially introduced as semi-empirical parameters, but a more complete understanding is now emerging and their application to solar cell analysis seems likely as illustrated in Section 4.9.

4.3 The High-Low Emitter

The high-low emitter structure has been proposed as a means for achieving increased emitter efficiency which would improve the open-circuit voltage of solar cells (Sah et al., 1978), and experimental results which appear to support the usefulness of this concept have been published (Neugroschel et al., 1978). On the other hand, attempts to demonstrate increased emitter efficiency by analytical methods or by numerical analysis of assumed high-low emitter junction profiles (unpublished work) have so far been unsuccessful; the emitter efficiency of the high-low structure has always been the same or inferior to that of the same emitter without the low region. Similar doubt has been expressed concerning the usefulness of high-low emitters in transistors (de Graaff and Slotboom, 1976). This is another area of solar cell investigation where further clarification is needed.

4.4 The J_{0n} Component of the Dark Saturation Current

The term involving J_{0n} in Equation 19 represents "excess current" which may have a variety of causes. Recombination in the transition region of the p-n junction (space-charge region recombination) is a well-known cause of exp (qV/nkT) behavior where $1 < n < 2$ (Lee and Nussbaum, 1980). Solar cell characteristics can often be decomposed into exp (qV/kT) and exp $(qV/2kT)$ components (Wolf et al., 1977; Wolf and Rauschenbach, 1963) and the latter is commonly attributed to space-charge region recombination (Hovel, 1973). Surface recombination has also been documented as a cause of $n = 2$ excess current in III-V semiconductor junctions (Henry et al., 1978).

Much higher n-values have also been reported, and these must have other origins. These forms of excess current may be caused by channels or inversion layers where the junction emerges at the semiconductor surface or by recombination at extended defects such as precipitate inclusions (Queisser, 1962; Sah, 1962).

4.5 Series Resistivity, R_s

The principal series resistance losses in the type of cell shown in Figure 5 come from the lateral flow of current in the N^+ layer and from the IR drop along the metal contact fingers. These cannot be completely

eliminated because they are involved in design compromises which determine the cell efficiency. Thus, a high collection efficiency and good blue response demand a thin N^+ layer, not too heavily doped, but this implies a high sheet resistance and a correspondingly high spreading resistance. To minimize grid shadow losses, the grid fingers must be made as narrow as possible without introducing too much resistance along their length. Other factors which may contribute to R_s, such as the metal-semiconductor contact resistance or bulk resistance in the base region, can be made negligible by proper cell design and fabrication methods and will not be dealt with here.

The equivalent circuit shown in Figure 6 cannot give an exact representation for these losses since the photocurrent is gathered from all over the surface of the cell and should therefore be represented by a distributed network. Nevertheless, the lumped constant equivalent circuit is very useful and gives sufficient accuracy for most purposes.

The equations describing cell characteristics have been expressed in terms of the current density, J, in order to keep the discussion independent of the cell area. Accordingly, R_s is expressed as the series resistivity with units of (ohm-cm^2). It is the product of the equivalent series resistance measured on a cell of any size multiplied by its area. R_s has the significance of a "figure of merit" since its value directly affects the curve factor. It is a measure of the success of a particular cell design in eliminating series resistance losses, independent of the area of the cell being evaluated. As a numerical illustration, a silicon cell with $R_s = 1$ ohm-cm^2 under 1-sun insolation suffers an efficiency loss of approximately 5% due to series resistance. A value of unity can thus be taken as the dividing point between efficient and inefficient cell designs.

The effects of series resistance can be characterized more generally by the dimensionless quantity

$$r = R_s J_{sc} / V_{oc} \tag{24}$$

(Green, 1977). This parameter provides a measure of cell quality which is independent of illumination intensity and the open-circuit voltage developed by the cell. The loss in curve factor due to series resistance is given approximately by

$$f = f_0 (1 - 1.1r) \tag{25}$$

where f_0 is the curve factor which would be obtained in the absence of series resistance. Equation 25 is valid for any value of light intensity and V_{oc}. The change in curve factor with series resistance is discussed further in Section 4.7.

The two principal contributions to R_s come from the spreading resistivity in the N^+ emitter layer, R_e, and the resistive drop along the grid wires, R_g. R_s is their sum,

$$R_s = R_e + R_g \tag{26}$$

An exact calculation of R_e requires a distributed network analysis which takes into account the difference in junction voltage between elements of the cell that are close to the grid contacts and those that are more remote. The latter are less heavily loaded and are therefore able to develop a higher voltage. Because of this they have a higher dark current and are not able to contribute as much photocurrent to the load.

A good approximation to R_e can be obtained by assuming that each element of the cell generates the same photocurrent density, J. R_e is evaluated by integrating the power dissipated by current flow in the emitter layer over the surface of the cell of area A. This loss is set equal to $I^2\mathcal{R}_e$ where $I = JA$ is the cell current and $\mathcal{R}_e$ is its series resistance. The resistivity is obtained by multiplying by the area of the cell, $R_e = \mathcal{R}_e A$.

This procedure will be illustrated by calculating the spreading resistivity associated with current collection by a set of parallel grid fingers spaced a distance d apart as shown in Figure 9. The fingers are assumed to be long enough that end effects can be neglected. We will take the unit cell of area $A = \ell d/2$ as a representative sample of the cell being analyzed. The current flowing toward the grid finger at a distance x from it is given by $J\ell\,(\frac{d}{2} - x)$ so the power dissipated in the emitter layer of the unit cell is given by

$$P_e = \int_0^{d/2} \left\{ J\ell \left[\frac{d}{2} - x \right] \right\}^2 \varrho_e \frac{dx}{\ell}$$

$$= J^2 \ell d^3 \varrho_e / 24$$

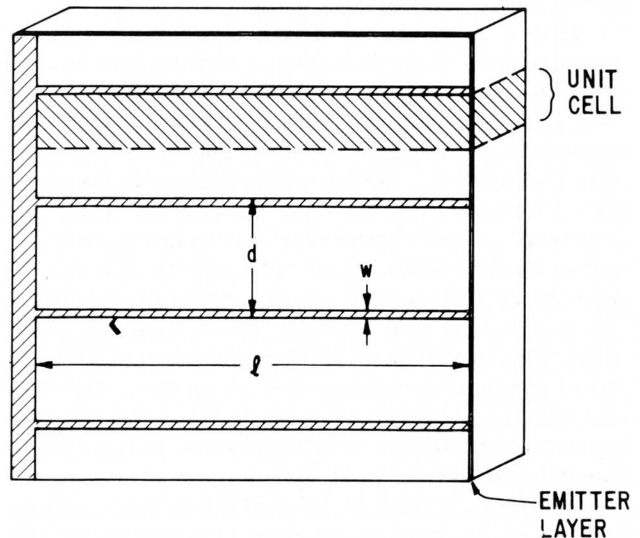

Figure 9. Solar cell with parallel grid fingers. It is assumed that $\ell >> d$ so end effects can be neglected.

where ϱ_e is the sheet resistance of the emitter layer. Setting $P_e = I^2\mathscr{R}_e = (J\ell d/2)^2\mathscr{R}_e$ gives $\mathscr{R}_e = \varrho_e d/6\ell$, so

$$R_e = \varrho_e d^2/12 \tag{27}$$

The corresponding formula for the resistivity introduced by the voltage drop along the grid fingers is

$$R_g = \varrho_m \ell^2 d/3w \tag{28}$$

where ϱ_m is the sheet resistance of the metal layer from which the grid fingers are formed and w is their width. A typical value for ϱ_m is 0.01 ohm/square for a metal layer a few microns thick. Equations 27 and 28 are smaller by a factor of 2/3 than the incorrect formulae that are often used for calculating R_s.

The fact that R_g increases with ℓ^2 places an important constraint on the maximum size of a cell having a front surface grid. As the cell is made larger an increasing fraction of its area must be covered with metal to conduct the current to the edge where it can be connected to the load.

Another method of contacting the emitter layer is to provide the cell with a two-dimensional array of feed-through paths to carry the photocurrent through the cell instead of across its front surface (Hall and Soltys, 1980). For feed-throughs of diameter b spaced a distance a apart the spreading resistivity associated with the emitter layer is

$$R_e = (\varrho_e a^2/2\pi)\{\ln(a/b) - 3/4\} \tag{29}$$

This cell design eliminates losses due to grid shadow and resistive drop along the grid fingers as well as the constraint on maximum cell size. On the other hand, a term similar to Equation 27 must be included to account for losses associated with the lateral flow of current in the substrate.

Several experimental methods have been used for measuring R_s. One procedure is to compare the dark J-V characteristic with a plot of J_{sc} vs V_{oc} measured at a series of different light intensities (Wolf and Rauschenbach, 1963). The latter represents the junction characteristic without any series resistance, so the difference between the two curves gives the JR_s drop. Another method of evaluating R_s is to observe the J-V characteristic under two different intensities of illumination, giving short-circuit currents J_{sc1} and J_{sc2}. The voltages V_1 and V_2 are noted where the current drops by the same amount ΔJ below the short-circuit values, and R_s is given by the ratio $(V_2 - V_1)/(J_{sc1} - J_{sc2})$. R_s can also be deduced from measurements of the diode admittance as a function of frequency (Chen et al., 1978).

Several experimental methods have been used for measuring R_s. One procedure is to compare the dark J-V characteristic with a plot of J_{sc} vs V_{oc} measured at a series of different light intensities (Wolf and Rauschenbach, 1963). The latter represents the junction characteristic without any series resistance, so the difference between the two curves gives the JR_s drop. Another method of evaluating R_s is to observe the J-V characteristic under two different intensities of illumination, giving short-circuit currents J_{sc1} and J_{sc2}. The voltages V_1 and V_2 are noted where the current drops by the same amount ΔJ below the short-circuit values, and R_s is given by the ratio $(V_2 - V_1)/(J_{sc1} - J_{sc2})$. R_s can also be deduced from measurements of the diode admittance as a function of frequency (Chen et al., 1978).

4.6 Shunt Conductance, G_{sh}

The low-voltage region of the J-V characteristic is often dominated by leakage current which flows across the junction along quasi-ohmic conduction paths. The current may result from any of several kinds of junction defects (Stirn, 1972) which need not be cataloged here. It is usually sufficient to represent the leakage by an ohmic term given by $G_{sh} = J/V$ evaluated at one or two tenths of a volt of forward bias where the "conductance hump" seen in Figure 7 dominates the J-V characteristic. Generally speaking, its magnitude should not exceed $\sim 10^{-3}$ mho/cm^2 to avoid a significant loss in cell performance. However, it should be emphasized that many of the leakage phenomena which contribute to G_{sh} are distinctly nonlinear so a precise evaluation of this parameter is seldom feasible.

4.7 Reduced Curve Factor Due to R_s and G_{sh}

The curve factor, defined by Equation 14, is determined by losses represented by R_s and G_{sh} of Equation 19 and by the effective n-value of the junction characteristic. Figures 10 and 11 show how the curve factor is reduced by the series resistance and shunt conductance, as calculated on the basis of the equivalent circuit of Figure 6. These curves assume an ideal junction characteristic ($n = 1$) at 300 K. They are expressed in terms of the dimensionless parameters r and g to make them applicable to cells of arbitrary area at any level of light intensity.

The curve factor will be reduced further if the J_{0n} component of the dark saturation current discussed in Section 4.4 is significant. This will decrease the curvature of the junction characteristic in a way that can be described by an effective n-value greater than unity, and result in a corresponding decrease in f (Green, 1977).

It may also be possible to have n-values smaller than unity. For example, in a junction where the dark current is determined by Auger recombination under high-level injection conditions the current would be proportional to the cube of the carrier concentration. This would lead to a current-voltage characteristic of the form $J \sim \exp(3qV/2kT)$, corresponding to $n = 2/3$.

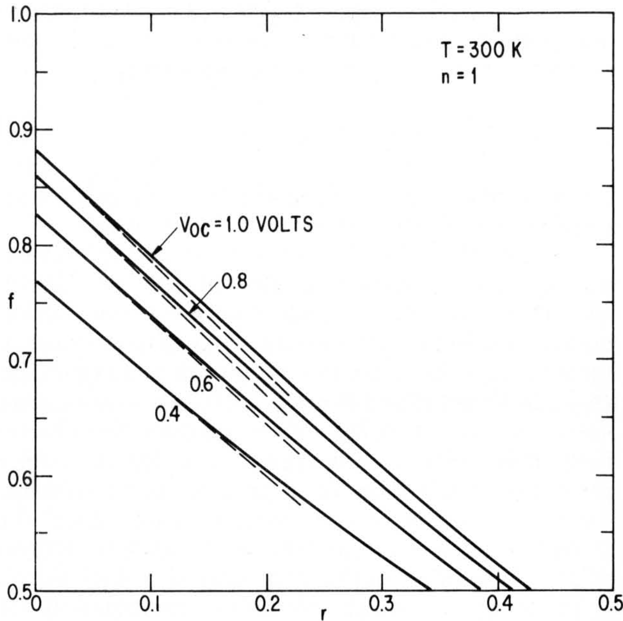

Figure 10. Change of curve factor with series resistivity parameter, $r = R_s J_{sc}/V_{oc}$. The dashed lines show the approximation given by Equation 25.

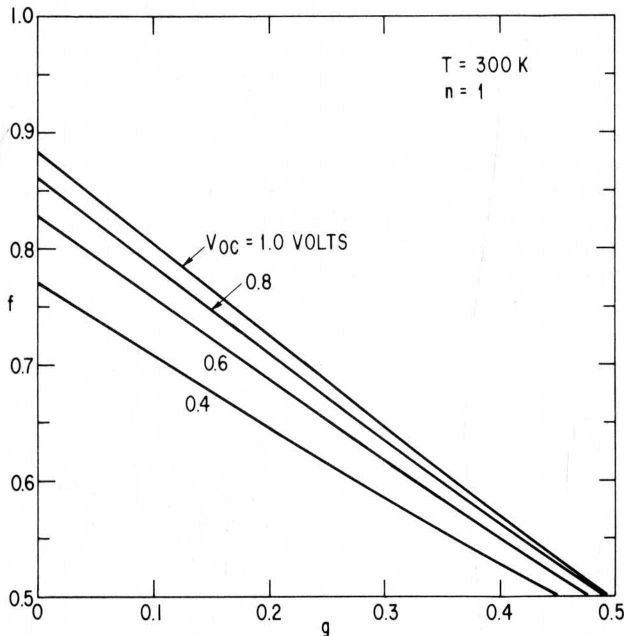

Figure 11. Change of curve factor with shunt conductance parameter, $g = G_{sh} V_{oc}/J_{sc}$.

4.8 Short-Circuit Current Density, J_{sc}

A general discussion of the photocurrent that can be realized in a silicon cell under AM1 insolation was presented above in Section 3.2. More detailed analyses of current collection in front surface junction cells of the form shown in Figure 5 have appeared (Hovel, 1975; Hauser and Dunbar, 1977; Fossum, Nasby, and Pao, 1980; Sze, 1969). These studies, confirmed by experimental measurements, have shown that it is possible to collect nearly all of the photogenerated carriers in a well designed and fabricated cell. The front junction must be very shallow, only one or two tenths of a micron deep; the diffusion length in the base must be greater than its thickness; and a back-surface field is needed to prevent recombination at the back of the cell.

Several measures have been introduced to reduce the optical losses. Texturing is beneficial in two respects. Combined with an antireflection layer, it yields a very low reflectivity over the entire useful portion of the solar spectrum (Arndt et al., 1975); also it refracts the light so that its path length within the silicon is greatly increased. Furthermore, any light that reaches the back of the cell will be totally reflected if this is a free silicon surface or if it has been suitably metallized, as in the back surface reflection (BSR) cell (Rasch et al., 1980; Wolf, 1980; Chai, 1980). Thus, the path length for optical absorption can be several times greater than the wafer thickness, significantly improving the red response of the cell. With these improvements in optical efficiency, grid shadowing remains as a principal limitation to the short-circuit current than can be realized in this type of cell. Grid shadow losses can be reduced in arrays which track the sun by using a saw-toothed cover slide to refract the light away from the metallized areas (Meulenberg, 1977).

4.9 Open-Circuit Voltage, V_{oc}

The open-circuit voltage developed by a solar cell depends upon the ratio of the short-circuit current to the dark saturation current as given by Equation 13. This equation requires some modification if significant nkT current exists near the operating point, but it is clear that the dark saturation current must be made as small as possible to achieve the maximum open-circuit voltage. The factors which contribute to J_{01} and J_{0n} were discussed above in Sections 4.2 and 4.4, and they have been treated extensively in the recent literature (Fossum et al., 1980; Lindholm and Fossum, 1980; Redfield, 1980; Shibib et al., 1979). An alternative treatment is given below to provide further insight into the factors which determine V_{oc}.

We will analyze the N^+-P-P^+ cell shown in Figure 8(b) with base thickness W assumed to be less than the electron diffusion length so the electron distribution will be substantially uniform throughout the base. The purpose of the calculation is to obtain an upper limit to V_{oc}, taking into account recombination in the base and minority carrier injection into the N^+ and P^+ end regions, but neglecting concentration gradients within the base region. The analysis will be formulated with arbitrary base doping P to make it applicable to both N^+-P-P^+ and N^+-I-P^+ cells and proceeds as follows. For given values of P and W,

we assume a series of values for the minority carrier concentration n and calculate the sum of the floating potentials at the N^+ and P^+ boundaries to obtain V_{oc}, with $p = P + n$ to maintain space-charge neutrality in the base. We also calculate the sum of the recombination and end region currents which gives J_{sc} and from it obtain the corresponding concentration ratio, C.

At equilibrium, the electron and hole concentrations are given by n_o and p_o. Under illumination both carrier concentrations increase and induce floating potentials at the two boundaries.

$$V_{N^+} = \frac{kT}{q} \ln\left[\frac{n}{n_o}\right]$$

$$V_{P^+} = \frac{kT}{q} \ln\left[\frac{p}{p_o}\right] = \frac{kT}{q} \ln\left[\frac{P+n}{p_o}\right]$$

V_{oc} is their sum,

$$V_{oc} = \frac{kT}{q} \ln\left[\frac{n(P+n)}{n_i^2}\right] \quad (30)$$

The base recombination per unit volume is given by $R = R_{\text{HSR}} + R_{\text{Auger}} + R_{\text{rad}}$ as discussed in Section 2.6. As a specific example of HSR recombination we will take $n_r = p_r = n_i$ and $\tau_{po} = \tau_{no} = \tau_{\text{HSR}}$. Since we are interested in electron concentrations in the range $n >> n_i$ we can drop terms in n_i^2 in the recombination functions, giving

$$R = \frac{n(P+n)}{\tau_{\text{HSR}}(P+2n)} + C_N n^2 (P+n)$$

$$+ C_P n (P+n)^2 + Bn(P+n) \quad (31)$$

The additional currents which are injected into the N^+ and P^+ regions will be calculated using the h-coefficient representation (Burtscher et al., 1975; Berz et al., 1979; Schlangenotto and Maeder, 1979). These coefficients were developed to provide a semi-empirical description of injection currents observed in transistors and P^+-I-N^+ rectifiers when operated under high-level conditions. Generalizing to make them applicable to both high and low-level injection as required in the present analysis, they yield end-region currents that are proportional to $(np-n_i^2)$ which has the same form as radiative recombination. Dropping the n_i^2 term gives,

$$J_{N^+} = qh_2 n (P+n)$$

and

$$J_{P^+} = qh_1 n (P+n) \quad (32)$$

for hole injection into the N^+ and electron injection into the P^+ regions respectively. We will take $h_1 + h_2 = 2 \times 10^{-14}$ cm^4/s to represent the lower range of values observed experimentally. The short-circuit current density is the sum of these components,

$$J_{sc} = qWR + J_{N^+} + J_{P^+} \quad (33)$$

Dividing this by an assumed value for J_{sc} under one-sun illumination gives the concentration ratio, C.

Figure 12 shows V_{oc} as a function of concentration ratio for a base doping of 10^{17} cm^{-3}, with $W = 0.02$ cm and $J_c = 40$ mA/cm^2 at one sun intensity. The upper curve assumes radiative recombinations alone, as in the analysis of Shockley and Queisser, 1961, and Ruppel and Wurfel, 1980. The open-circuit voltage at one sun (0.765 volt) is less than the radiative limit (0.84 volt) since it applies to a specific device geometry rather than to a general thermodynamic limit. Including Auger recombination gives the second curve, which represents a cell made from ideal silicon, free of recombination centers. Real silicon contains defects which promote recombination via energy levels close to the middle of the energy gap. Taking $\tau_{\text{HSR}} = 50$ μs as representative of high quality silicon after processing into a solar cell gives the third curve. This curve represents cell performance that might be achievable if injection into the end regions could be eliminated. So far no way has been found to accomplish this so a fourth curve has been calculated, including all of the above recombination processes and using the h-coefficients to allow for additional dark current due to injection into the N^+ and P^+ regions. This curve corresponds to current state-of-the-art cell technology. The difference between curves 3 and 4 can be regarded as a "technology gap." It represents the improvement in V_{oc} that might be achievable if the excess dark current could be eliminated.

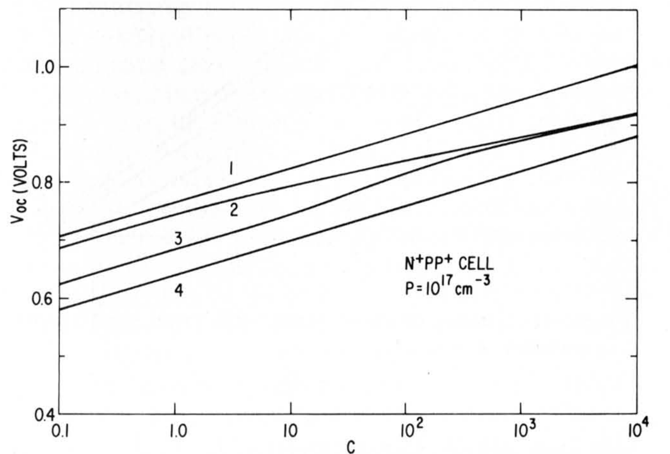

Figure 12. Open-circuit voltage vs concentration ratio for base doping of 10^{17}cm^{-3}. Curve 1: Radiative recombination (RR) only; curve 2: RR + Auger recombination; curve 3: RR + Auger + HSR; curve 4: RR + Auger + HSR + h-coefficient injection.

Figure 13 shows the corresponding behavior calculated for the P^+-I-N^+ cell, to be discussed in Section 6. Curve 1, which assumes radiative recombination alone, is identical. The others are all lower except for the low concentration end of curve 2. At very high concentration ratios the curves of Figures 12 and 13 coincide since the base region impurities of the N^+-P-P^+ cell are overwhelmed by the free carriers.

N^+-P-P^+ cell performance corresponding to curves 3 and 4 is shown in Figure 14 as a function of base region impurity concentration for several values of incident light intensity. The regions of high-level (HL) and low-level (LL) operation are indicated by a diagonal line. V_{oc} is independent of base doping in the HL region. The curves pass through broad maxima in the 10^{17} cm^{-3} doping range as observed experimentally. However, to bring these maxima into agreement with observed V_{oc} values it is necessary to include the excess dark current due to injection into the end regions as shown by the dashed curves. The factors which contribute to this excess current are not adequately understood at present. They include the heavy doping effects discussed in Section 2.2, and any shunt conductance, edge leakage, and *nkT* current that may be present in actual cells.

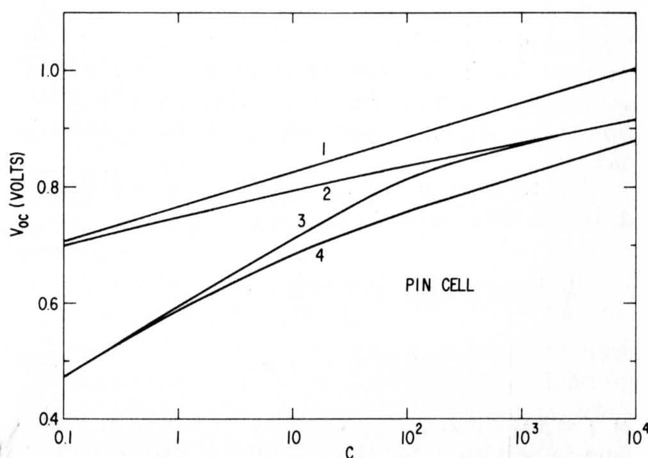

Figure 13. Open-circuit voltage vs concentration ratio for the P^+-I-N^+ cell. Curves 1 to 4 as in Figure 12.

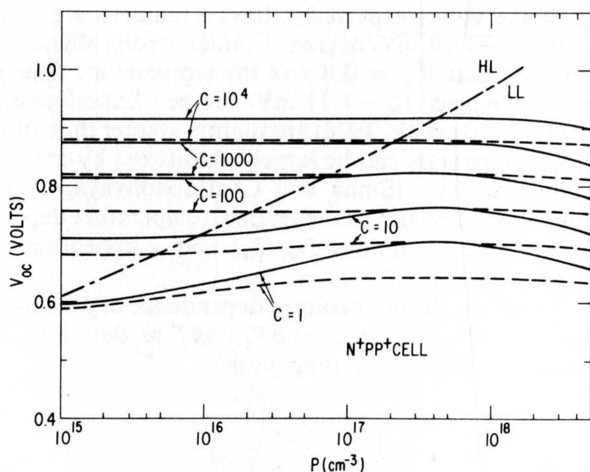

Figure 14. Open-circuit voltage vs base region acceptor concentration for N^+-P-P^+ cell, for various optical concentration ratios. Solid curves assume radiative, Auger, and HSR recombination. Dashed curves include *h*-coefficient injection into the end regions. The diagonal line delineates regions of high-level and low-level operation.

4.10 Efficiency, η

The efficiency for converting incident solar radiation into electrical power is given by the ratio, $\eta = P_{out}/P_{in} = fJ_{sc}V_{oc}/P_{in}$. The maximum achievable efficiency for a silicon cell under one sun illumination is determined by many fundamental and technological factors as discussed in the preceding sections. One of the more elusive of these is the actual spectral distribution assumed, which we will take to be that of the AM1 spectrum with a correction factor applied to make the total incident power, P_{in} = 1 kW/m^2. With this illumination we estimated in Section 3.2 that the maximum possible short-circuit current would be 45 mA/cm^2 for an arbitrarily thick cell ($W = \infty$) and 40 mA/cm^2 for one with a more realistic value for the effective thickness ($W \approx 200$ microns). Corresponding values for the open-circuit voltage as calculated in the preceding section and taking the curve factor from Figure 4 are summarized in Table 1. The last column gives the cell efficiency. Also included in this table is the highest efficiency cell calculated by Wolf in his analysis of the "limit efficiency" for silicon cells under similar insolation (Wolf, 1980). From this tabulation it would appear that efficiencies approaching 22 to 24% might be achievable, depending upon the success of efforts to reduce the excess dark current and grid shadow losses.

There has been steady progress in this direction in recent years. Efficiencies in the 17 to 18% range have been reported for laboratory results, while those of commercial cells have reached 14 to 16%. The latter are limited by cost constraints, silicon crystal quality, and the inertia of placing new technology into operation.

4.11 Temperature Dependence

The discussion so far has dealt with cell performance near room temperature, T_{rt} = 300 K. Operation at higher temperatures is often required so we need to consider how the characteristics are affected by changes in cell temperature.

The temperature coefficient of efficiency is defined by

$$\beta = -\frac{1}{\eta}\frac{d\eta}{dt}$$

$$= -\frac{1}{f}\frac{\partial f}{\partial T} - \frac{1}{J_{sc}}\frac{\partial J_{sc}}{\partial T} - \frac{1}{V_{oc}}\frac{\partial V_{oc}}{\partial T} \quad (34)$$

so at a temperature difference ΔT above room temperature the efficiency will be given to first order by

$$\eta \sim \eta_{300}(1 - \beta \Delta T) \quad (35)$$

We wish to evaluate β at 300 K in a way that shows its functional dependence upon the cell parameters.

Table 1

MAXIMUM EFFICIENCY FOR N^+-P-P^+ SILICON CELLS WITH $n=1$ AND $T=300$ K

AM1 insolation with P_{in} = 1 kW/m^2

Cell Conditions	J_{sc} (mA/cm^2)	V_{oc} (Volts)	f	η
W = ∞; $h_1 = h_2 = 0$	45	.708	.847	27.0
W = 200μ; $h_1 = h_2 = 0$	40	.705	.846	23.9
W = 200μ; $h_1 h_2 > 0$*	40	.643	.836	21.5
Limit efficiency†	39.1	.749	.853	25.2

*$h_1 + h_2 = 2 \times 10^{-14}$ cm^4/s.
†Wolf, 1980 (Table III, best cell).

The short-circuit current is almost unaffected by temperature. Most of the photogenerated carriers are produced close to the junction and are collected. Those that must diffuse a significant distance to reach the junction are subject to recombination losses, but these are rather insensitive to changes in temperature. The decrease in energy gap with temperature gives rise to the small positive temperature coefficient expressed by Equation 18.

The open-circuit voltage, given by Equation 13, involves the dark current, J_{01}. This may take several forms depending upon the cell constructions, as expressed by Equations 22 and 23, but in all cases the principal temperature dependence is contained in the n_i^2 factor which increases rapidly with temperature as described by Equation 2. Neglecting the temperature dependence of the other coefficients, we can write Equation 13 in the form $V_{oc}(T) = (kT/q)\ln(\text{const}/n_i^2)$. Subtracting its value at $T = T_{rt}$ and using (2) gives (Hu and Drowley, 1978),

$$V_{oc}(T) = V_{rt} - (E_{g0}/q - V_{rt})\left[\frac{T}{T_{rt}} - 1\right] - \left[\frac{3kT}{q}\right]\ln\left[\frac{T}{T_{rt}}\right] \quad (36)$$

where V_{rt} is the open-circuit voltage at room temperature, T_{rt}. The last term in Equation 36 is generally much smaller than the others. Neglecting it, we obtain the useful approximation,

$$V_{oc}(T) \approx V_{rt} - (E_{g0}/q - V_{rt})\left[\frac{T}{T_{rt}} - 1\right] \quad (37)$$

This equation describes the linear decrease of V_{oc} with temperature that is commonly observed, and shows how it depends upon V_{rt} and the energy gap of the semiconductor. V_{oc} vanishes at a temperature T_0 given by

$$T_0 = \frac{T_{rt}}{(1 - qV_{rt}/E_{g0})} = \frac{T_{rt}}{1 - V_{rt}/1.21} \quad (38)$$

For example, a cell with V_{oc} = 0.6 volt at room temperature would be expected to have its open-circuit voltage fall to zero at 295 °C. Under strong illumination such that V_{oc} = 0.8 volt, T_0 would increase to 585 °C.

The temperature coefficient of V_{oc} is obtained by differentiating Equation 36, giving

$$\frac{\partial V_{oc}}{\partial T} = -(E_{g0}/q + 3kT/q - V_{oc})/T = -(1.133 - V_{oc})/300 \quad (39)$$

at $T = 300$ K, since $E_{g0} = 1.210$ eV. It will be shown later in Section 6 that this equation is also correct for the P^+-I-N^+ cell, where $n = 2$. Equation 39 shows that a cell with a low open-circuit voltage will have greater temperature dependence than one with a large V_{oc}. For example, a cell under one-sun insolation with V_{oc} = 0.6 volt is expected to have a temperature variation of -1.78 mV/degree. Under strong illumination such that V_{oc} = 0.8 volt the temperature dependence is reduced to -1.11 mV/degree. Experimental results (Castle et al., 1978) are slightly greater than this. The discrepancies can be largely eliminated by a more detailed analysis (Sinha and Chattopadhyaya, 1979) which takes account of the gradual temperature dependence of the quantities D_e, L_e, and τ appearing in Equations 22 and 23.

To obtain the temperature dependence of f we note that $f = f(U)$, where $U = qV_{oc}/nkT$ as described in Section 3.1. Differentiating gives

$$\frac{\partial f}{\partial T} = \frac{1}{nkT}\left[\frac{\partial V_{oc}}{\partial T} - \frac{V_{oc}}{T}\right]\frac{\partial f}{\partial U} = -\frac{E_{g0} + 3kT}{nkT^2}\frac{\partial f}{\partial U} = -\frac{1.133}{nkT^2}\frac{\partial f}{\partial U} \quad (40)$$

Combining this result with Equations 18, 34, and 39 gives

$$\beta = \frac{E_{g0} + 3kT}{T}\left[\frac{1}{nkTf}\frac{\partial f}{\partial U} + \frac{1}{V_{oc}}\right]$$

$$- \frac{1}{T} - 3 \times 10^{-4}$$

$$= \frac{0.1461}{nf}\frac{\partial f}{\partial U} + \frac{0.00378}{V_{oc}} - 0.00363 \qquad (41)$$

at $T = 300$ K. As noted above, this equation is valid for both $n = 1$ and 2. Using f and $\partial f/\partial U$ from Figure 4 gives the dependence of β on V_{oc} shown in Figure 15. It accounts quite accurately for the observed behavior of silicon cells as functions of temperature and optical concentration (Burgess and Fossum, 1977; Castle et al., 1978; Frank et al., 1980).

Equation 41 can be applied to cells made from other semiconductors by using corresponding values for E_{g0} and the term (-3×10^{-4} deg^{-1}) which comes from Equation 18 and accounts for the change in optical absorption edge with temperature.

5. OTHER CELLS WITH FRONT SURFACE COLLECTING JUNCTIONS

Photovoltaic energy conversion does not necessarily require the formation of a p-n junction. Schottky barrier cells are made by depositing a thin, nearly transparent, metal layer on the front surface of an n- or p-type wafer. Current collection and charge separation are achieved by the space-charge field at the metal-semiconductor interface in a manner analogous to that in a p-n junction cell. The open-circuit voltages tend

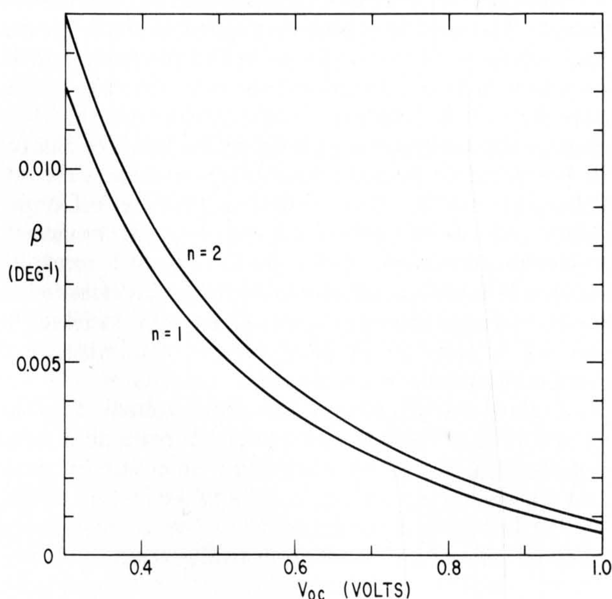

Figure 15. Temperature coefficient of cell efficiency vs open-circuit voltage.

to be lower, however, because the barrier height is limited by Fermi-level pinning at the semiconductor surface, and this form of cell appears to be of limited value for power generation purposes.

A closely related cell employs a degenerate semiconductor layer such as indium-tin-oxide in place of the metal. In either case, the metal or degenerate semiconductor layer must contain enough free carriers per unit area to permit current collection without excessive spreading resistance loss, so there will be a corresponding optical transmission loss due to free-carrier optical absorption. The ratio of sheet conductance to optical absorption is determined principally by the relaxation time for free carrier scattering so it is not immediately evident that transparent semiconductors have any spreading resistance advantage over thin metal layers, and both have been used with comparable success.

The open-circuit voltages of these cells can be markedly improved by including a thin insulating layer between the conducting layer and the semiconductor. These structures are called metal-insulator-semiconductor (MIS) and semiconductor-insulator-semiconductor (SIS) cells, respectively. The insulator must be thin enough (~15 to 20 Å) to permit the flow of tunnel current without a significant voltage drop. Its principal function seems to be the elimination of Fermi-level pinning at the surface of the semiconductor so that larger barrier heights can be achieved. These structures and other modifications which have contributed to increased efficiencies are discussed below.

5.1 MIS and SIS Cells

The theoretical understanding and current status of MIS and SIS cell development have been reviewed recently (Shewchun, Burk, and Spitzer, 1980; Ng and Card, 1980). Two modes of operation can be distinguished. With modest barrier heights the dark current is dominated by majority carrier transport as is typical for Schottky barriers on silicon. However, in Al-SiO_2-pSi cells the silicon surface can be so strongly inverted that the dark current is determined by minority carrier flow as in a p-n junction cell. Minority carrier MIS cells have shown slightly higher efficiencies than majority carrier cells, but they require very thin I-layers (~10 Å) where direct contact between the aluminum and silicon is difficult to avoid.

One of the principal advantages of all of these cells is their structural simplicity and ease of fabrication. Furthermore, degradation of the silicon quality, which often results from high-temperature process steps, can be avoided. Efficiencies in the range 10 to 12% have been reported, limited largely by their open-circuit voltages which tend to be significantly lower than those of p-n junction cells.

One of the unresolved questions concerning these cells is their long-term stability (Kleta and Pulfrey, 1980; Godfrey and Green, 1979). It is not clear whether the integrity of an oxide layer only about 15 Å thick can be maintained under the environmental conditions that will be encountered in field applications.

5.2 Oxide Charge-Induced Inversion Layer Cells

An electric field applied to the surface of a semiconductor can be used to attract minority carriers to the surface, producing an inversion layer with electrical characteristics similar to those of p-n junctions. Inversion layers produced by dielectric layers containing built-in positive or negative charges (electret layers) offer important advantages in photovoltaic applications. The reduction in V_{oc} caused by heavy doping effects is eliminated since the inversion layer does not depend upon impurities being present in the semiconductor itself. Indeed, the open-circuit voltages achieved with inversion layer cells (V_{oc} = 0.642 V at AM1, 28 °C) are among the highest reported for any silicon cell (Godfrey and Green, 1980). A further advantage is that the inversion layer is only about 1000 Å thick and has a strong electric field, oriented to drive minority carriers toward the junction instead of being weakened or possibly inverted by band-gap narrowing. This contributes to good collection efficiency, particularly at the blue end of the spectrum. The principal limitation of these cells is set by the number of charges per unit area that can be induced in the inversion layer. Values in excess of 10^{12} cm^{-2} are difficult to achieve, leading to inversion layer sheet resistances in excess of 20,000 ohms per square.

Charged dielectric layers can be formed by low temperature CVD of SiO_x (Theriault and Thomas, 1978) or by annealing thermally grown SiO_2 in oxygen at low temperatures (Deal et al., 1967). Spin-on tantalum oxide has also been reported to induce strongly inverted layers on p-type silicon and good cell performance has been achieved (Thomas et al., 1980).

Oxide charge induced layers can be incorporated in solar cells in several ways. When used as the I-layer of an MIS or SIS cell they give rise to increased barrier heights which can result in improved efficiency and minority carrier dominated dark current characteristics. The grating structure inversion layer cell utilizes a metal grid which makes electrical contact with the inversion layer by tunneling through a thin oxide layer. This form of cell has achieved AM1 efficiencies of 17 to 18 percent for converting the radiation which falls on the unshadowed portion of the cell surface (Godfrey and Green, 1980; Thomas et al., 1980). However, because of the high sheet resistance of the inversion layer, it has been necessary to apply as many as 10 grid lines/mm to achieve an acceptably low series resistance loss and the efficiency referenced to the total cell area is substantially less.

Charged oxide layers can also be used to enhance the emitter efficiency of p-n junction cells by suppressing surface recombination at the front surface of the cell (Neugroschel et al., 1978). They have also been suggested as a way of forming accumulation layers to serve as the BSF contact of a P^+-N-N^+ cell, with the potential for low effective surface recombination and reduced dark current associated with that contact (Neugroschel, 1980; Tarr et al., 1980).

5.3 Double-Sided Junction Cells

Various forms of p-n junction cells have been reported which have collecting junctions on both sides of the wafer. An early version of this configuration was proposed as a space cell which would have increased radiation damage resistance (Capart, 1968). More recently, a double-sided cell has been developed for terrestrial application where both faces of the cell would be illuminated (Chambouleyron and Chevalier, 1977).

The tandem junction cell is another double-sided cell, designed to operate with the front junction floating (Chiang et al., 1978). This junction serves as a reflecting surface for the photogenerated minority carriers which must diffuse to the back junction to be collected. This design eliminates the front-surface grid and provides a planar front surface with all of the metallization on the back which simplifies encapsulation. On the other hand, the loss of carriers by bulk recombination tends to be high since most of the generation occurs near the front surface so the carriers must diffuse across the cell to the back to be collected. This shortcoming has been eliminated in the polka dot cell by providing a multiplicity of interconnection paths to carry the current collected at the front junction through the cell to the back so efficient collection can be achieved at both junctions (Hall and Soltys, 1980).

6. P^+-I-N^+ CELLS

One of the simplest concepts for a photovoltaic cell consists of a wafer of intrinsic semiconductor with N^+ and P^+ contacts formed within a diffusion length of each other. Upon exposure to light, the photogenerated electrons and holes diffuse to these contacts where they are selectively captured to generate the electrical output of the cell.

Silicon P^+-I-N^+ cells have been made in two distinct forms. The junctions may be applied to the front and back surfaces of the wafer as in the conventional cell geometry with its front-surface grid, shown in Figures 5 and 8 (Meulenberg et al., 1980). Alternatively, both junctions may be applied to the back of the cell in the form of interdigitated fingers (Lammert and Schwartz, 1977). This Interdigitated Back Contact (IBC) cell offers several advantages, particularly at high concentration. Grid shadowing and spreading resistance losses in the shallow emitter layer are eliminated. Furthermore, the undoped front surface of the cell is more easily passivated to minimize losses caused by surface recombination.

Equation 15 describes the photovoltaic behavior of the P^+-I-N^+ cell in its idealized form where terms representing series resistance and injection into the end regions have been neglected and a constant minority carrier lifetime is assumed. The corresponding open-circuit voltage, analogous to Equation 13, is

$$V_{oc} = \frac{2kT}{q} \ln (J_{sc}/J_{02} + 1) \approx \frac{2kT}{q} \ln (J_{sc}/J_{02}) \qquad (42)$$

The factor of 2 in the prefactor of this equation is often taken to mean that higher open-circuit voltages can be expected in P^+-I-N^+ cells than for cells made from extrinsic material, where Equation 13 applies (Meulenberg et al., 1980). This is a misconception, however; J_{02} is always so much larger than J_{01} that the open-circuit voltage of a P^+-I-N^+ cell is always less than that of a similar cell formed with an extrinsic base region. This can be seen by considering the origin of Equation 15. Under forward bias conditions $n = p = n_i \exp(qV/2kT)$ and the dark current term is equal to the recombination rate, Equation 6, integrated over the volume of the I-region. If V is large enough that the lifetime becomes constant and equal to the high-level lifetime given by Equation 8, then this term becomes $(qWn_i/\tau_\infty)\exp(qV/2kT)$, so

$$J_{02} = qWn_i/\tau_\infty \qquad (43)$$

The difference in the voltages developed by the two kinds of cell is obtained by subtracting Equation 13 from Equation 42, giving

$$V_{oc}(P^+\text{-I-}N^+) - V_{oc}(N^+\text{-P-}P^+)$$

$$= (kT/q)\ln(J_{01}J_{sc}/J_{02}^2).$$

It can only be positive if $J_{01}J_{sc}/J_{02}^2$ is greater than unity. Since $J_{sc} = qnW/\tau$, we obtain using Equations 23b and 43,

$$\frac{J_{01}J_{sc}}{J_{02}^2} = \frac{n\tau_\infty^2}{N_A\tau^2} \qquad (44)$$

Under low-level conditions this ratio is dominated by n/N_A which is small compared with unity by definition, so the open-circuit voltage of the P^+-I-N^+ cell must always be less than that of the N^+-P-P^+ cell. (Obviously, the same conclusion holds for comparison with a P^+-N-N^+ cell.) Under high-level conditions, N_A is swamped by the free carriers and the different cell types become indistinguishable. This conclusion is born out by the curves of Figures 12 and 13. The cells in these examples assumed the same structures and recombination processes, but V_{oc} was always less for the P^+-I-N^+ cells throughout the range of low-level operation and identical beyond.

The temperature dependence of V_{oc} is obtained by differentiating Equation 42, with J_{02} given by Equation 43. Since τ_∞ is assumed to be constant, the only temperature dependent quantity in Equation 43 is n_i. When these two equations are combined the result is exactly the same as that given by Equation 39. In other words, for the same open-circuit voltages (which may require different illumination intensities) the temperature coefficient of V_{oc} is the same for the P^+-I-N^+ cell as for the N^+-P-P^+ cell.

It should also be noted that the form $[\exp(qV/2kT) - 1]$ in Equation 15 cannot be expected to hold near $V = 0$ because of the nonlinear behavior of the recombination rate, Equation 6, in this region. The (-1) term is meaningless, and was only introduced as a formal convenience to make the dark current vanish at $V = 0$. It is only when V becomes large enough to achieve a constant high-level lifetime that the $\exp(qV/2kT)$ behavior of Equation 15 can be expected to hold.

The theoretical curve factor is also less for the ideal P^+-I-N^+ cell because of its larger n-value. For operation at 300 K with $V_{oc} = 0.6$ volt and $n = 2, f = 0.721$ compared with 0.827 for a cell with $n = 1$, as shown in Figure 4. I-V characteristics corresponding to $n = 2$ are seldom actually observed in P^+-I-N^+ cells because of the complicating effects of injection into the end regions and the onset of Auger recombination as high-level injection is reached. For example, the edge-illuminated cell discussed in the following section (Frank et al., 1980) is constructed as a P^+-I-N^+ cell but displays $n = 1$ behavior over most of its operating range.

A more detailed analysis of the P^+-I-N^+ cell requires taking into account additional losses such as those caused by series resistance and injection into the end regions. For cells having contacts applied to opposite faces of the I-region the analysis parallels that presented above for the N^+-P-P^+ cell, and will not be developed further here. An interesting numerical simulation and proposed experimental study of a P^+-I-N^+ cell with field-induced junctions has recently been described (Chappel, 1980). Valuable insight is also provided by studies of power rectifiers and thyristors (Spenke, 1968; Berz, 1977; Berz et al., 1979; Burtscher et al., 1975; Schlangenotto and Maeder, 1979).

The IBC cell has the advantage of a greatly reduced series resistance since the collected current is not required to flow laterally through a thin surface layer. Its analysis is more difficult, however, and most treatments have resorted to numerical methods (Lammert and Schwartz, 1977; Chin and Navon, 1980).

7. EDGE-ILLUMINATED MULTIJUNCTION CELLS

The cells discussed thus far have had the form of flat wafers with junctions parallel to their major surfaces, so the illumination is presumed to be incident more or less perpendicular to the plane of the junctions. It is possible to imagine a planar N^+-P-P^+ cell cut into narrow strips which are turned 90° and reassembled to form a composite wafer having many subcells connected in series as illustrated in Figure 16(a).

Multijunction cells such as these have several attractive features. The front surface grid with its shadowing and resistive losses is eliminated. Most of the front surface consists of low-doped silicon which can have a long minority carrier lifetime and is easily passivated to yield a low surface recombination velocity.

A further advantage is that the subcells are connected in series, so the output is delivered at a more convenient impedance for interconnection with the rest of the electrical system.

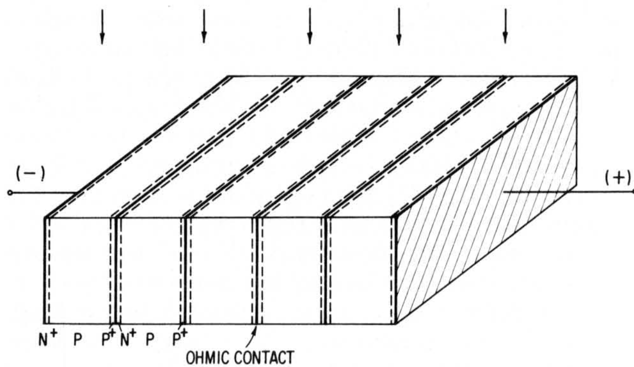

(a) Edge-illuminated multijunction cell

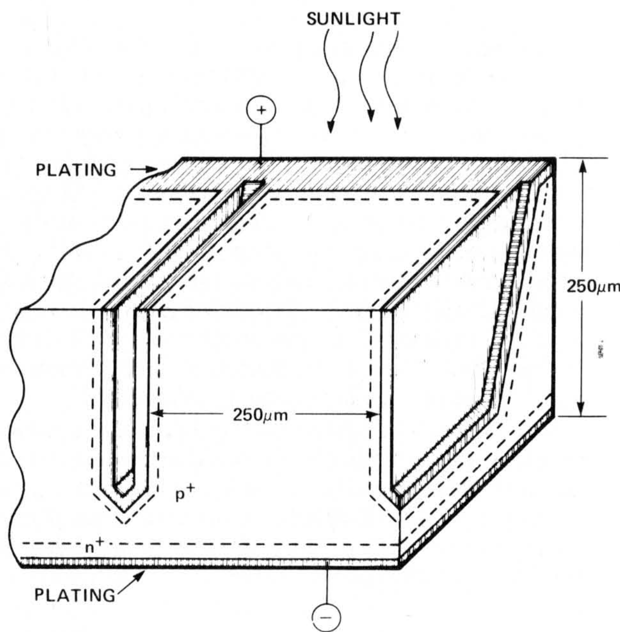

(b) Selectively etched multijunction cell (Frank et al., 1980)

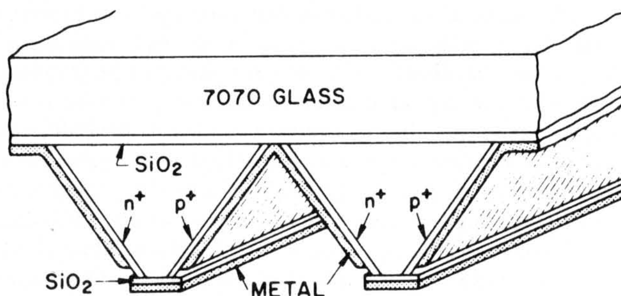

(c) *V*-groove multijunction cell (Chappel, 1979)

Figure 16. Examples of edge-illuminated multijunction cells.

This form of cell also has disadvantages which should be recognized. The illumination must be uniform over its surface since the current generated by the composite cell will be limited to the lowest current produced by any of its subcells. This can be a serious constraint in many forms of optical concentration systems. The ohmic connection layer and the adjoining N^+ and P^+ layers give rise to optical and electrical "dead layer" losses which can be as large as the grid shadow losses of a conventional cell. Finally, there are serious technical problems with forming the composite cell with subcells that are less than a diffusion length in thickness without degrading their electrical properties.

The analysis of edge-illuminated cells is made difficult by the varying optical generation rate with distance from the illuminated surface of the cell, so this variation has not been taken into account in currently available analyses (Goradia and Sater, 1977). Experimentally, efficiencies of barely 8% at concentration ratios of several hundred have been reported for the cell structure shown in Figure 16a (Goradia and Goradia, 1976).

A different form of edge-illuminated cell has been made by the anisotropic etching of <110> oriented silicon wafers (Wohlgemuth and Scheinine, 1980; Frank et al., 1980). An example of a cell produced by this method is shown in Figure 16(b). The front surface of the lightly doped ($\sim 10^{14} cm^{-3}$) n-type wafer is selectively etched to produce an array of very narrow grooves which are then diffused to form shallow P^+ collecting junctions. These are contacted by electroplated metal conductors which are joined together by a bus conductor along the edges of the cell. The cell functions much like a planar P^+-I-N^+ cell, where the P^+-diffused grooves correspond to the front junction and the electroplated conductors correspond to the grid. However, since the groove metallization is tipped up on edge, it can cover the entire collection surface without intercepting any more light. Thus, R_s can be made very low. An efficiency of 17.6% has been reported at a concentration ratio of 500 suns (Frank et al., 1980). This cell generates a high current at low voltage since all of its junctions are connected in parallel. On the other hand, unlike a series-connected multijunction cell, its efficiency is almost unaffected by nonuniform illumination.

Many other junction configurations are possible, as exemplified by the V-groove multijunction cell shown in Figure 16(c) (Chappel, 1979). Like most of the other multijunction cells, this one is designed for operation at high optical concentration ratios. It is a series-connected P^+-I-N^+ cell whose 3-dimensional structure is produced by anisotropic etching, with ion implantation to form the alternating p-n junctions. This method of construction requires that the cell be bonded to a glass superstrate throughout the fabrication sequence. It offers good environmental protection but makes it difficult to eliminate losses due to front-surface optical reflection.

8. CONCLUDING REMARKS

This report has dealt primarily with the analysis and physical understanding of silicon photovoltaic cells and has emphasized approaches which could be used to achieve the highest possible operating efficiency. Much of the treatment assumed high-quality, single-crystal silicon, often with selected crystallographic orientation. These issues are of paramount importance in concentrator applications where the cell amounts to only a small fraction of the total system cost, but they play a lesser role in determining power generation costs in flat panel arrays where emphasis must be placed upon achieving very low cell fabrication costs, consistent with reasonable operating efficiency.

Some recent developments concerning the cost of silicon solar cells for terrestrial power generation deserve mention. Further evaluation of several approaches to the manufacture of low-cost solar grade polycrystalline silicon indicates that cost reductions by a factor of five or more compared with present polysilicon costs should be possible (Yaws et al., 1980 and references therein). Progress in the preparation of low-cost sheet silicon by the Czochralski and heat exchanger methods and the casting of large-grain polycrystalline ingots was reported at the 14th Photovoltaic Specialists Conference, but it still is not clear which of these approaches would yield the lowest power generation costs if carried to maturity. Continuous float-zone or pedestal growth would appear to show promise for the manufacture of low-cost single-crystal silicon by eliminating crucible expense and contamination and the difficulties caused by SiO evolution during growth, but these approaches have received little attention so far.

The foregoing ingot growth methods must all contend with the problem of slicing the ingot into wafer form, which constitutes a substantial component in the cost of the finished cell. Slicing is avoided by the ribbon growth methods such as EFG (Kalejs et al., 1980) and dendritic web (Duncan et al., 1980). These have been joined recently by roller quenching (Tsuya et al., 1980) which has produced fine-grained silicon ribbon at velocities as high as 40 m/s. Cells made from these ribbons have been reported to have AM1 efficiencies of 5%, which must be considered as encouraging at this early stage of development.

The economic issues which will determine the choice of cell technology and their application to terrestrial power generation are complex and could not be addressed in this report. They have been discussed in the recent book by Johnston, 1980, and by the APS Study Group on *Solar Photovoltaic Energy Conversion* of which this author was a member, and reference is made to their report (Ehrenreich et al., 1979).

BIBLIOGRAPHY

"Solar Cells," edited by C.E. Backus, *IEEE Selected Reprint Series* (1976).

"Solar Cells," by H.J. Hovel, Volume 11 of *Semiconductors and Semimetals*, Academic Press (1975), edited by R.K. Willardson and A.C. Beer.

Solar Voltaic Cells, by W.D. Johnston, Jr., Marcel Dekker, 1980.

Photovoltaic Power Generation, by D.L. Pulfrey, Van Nostrand Reinhold Co., 1978.

Proceedings of the IEEE Photovoltaic Specialists Conferences, held at 18-month intervals. The latest was the 14th PVSC, held in San Diego in January 1980.

Proceedings of the (European) Photovoltaic Solar Energy Conferences, also held at 18-month intervals. Recent PSEC meetings were held in Luxembourg (October 1977), Berlin (April 1979), and Cannes, France (October 1980).

Special issues of the IEEE Trans. Electron Devices devoted to Photovoltaic Cells: ED-24 (April 1977) and ED-27 (April 1980).

Solar Cell Array Design Handbook: The Principles and Technology of Photovoltaic Energy Conversion, by Hans S. Rauschenbach, Van Nostrand Reinhold Co., 1980.

REFERENCES

Abram, R.A., Rees, G.J., and Wilson, B.L.H., 1978, *Adv. Phys. 27,* 799, "Heavily Doped Semiconductors and Devices."

Amantea, R., 1980, *IEEE Trans. Electron Devices ED-27,* 1231, "A New Solution for Minority-Carrier Injection into the Emitter of a Bipolar Transistor."

Arndt, R.A., Allison, J.F., Haynos, J.G., and Meulenberg, A., 1975, Proc. 11th Photovoltaic Specialists Conf., p. 40, "Optical Properties of the Comsat Non-reflective Cell."

Baliga, B.J., 1980, Appl. Solid State Sci. Suppl., R. Wolfe, ed., Academic Press, NY, *Silicon Power Field Controlled Devices and Integrated Circuits* (to be published).

Barber, H.D., 1967, *Solid-State Electron. 10,* 1039, "Effective Mass and Intrinsic Concentration in Silicon."

Berz, F., 1977, *Solid-State Electron. 20,* 709, "A Simplified Theory of the p-i-n Diode."

Berz, F., Cooper, R.W., and Fagg, S., 1979, *Solid-State Electron. 22,* 293, "Recombination in the End Regions on PIN Diodes."

Bludau, W., Onton, A., and Heinke, W., 1974, *J. Appl. Phys. 45,* 1846, "Temperature Dependence of the Band Gap of Silicon."

Burgess, E.L. and Fossum, J.G., 1977, *IEEE Trans. Electron Devices ED-24,* 433, "Performance of n^+-p Silicon Solar Cells in Concentrated Sunlight."

Burtscher, J., Dannhauser, F., and Krausse, J., 1975, *Solid-State Electron. 18,* 35, "Die Rekombination in Thyristoren und Gleichrichtern aus Silizium: Ihr Einfluss auf die Durchlasskennlinie und Das Freiwerdezeitverhalten."

Capart, J.J., 1968, European Space Research Organization Technical Note ESRO TN-3, November 1968, "Design of Solar Cells with Two Collecting Junctions."

Castle, J., Payne, P., Aerni, E., and Stella, P., 1978, Proc. 13th Photovoltaic Specialists Conf., p. 810, "Test and Evaluation of Silicon Cells Optimized for High Efficiency under Concentrated Sunlight."

Chai, A.-T., 1980, Proc. 14th Photovoltaic Specialists Conf., p. 156, "Back Surface Reflectors for Solar Cells."

Chambouleyron, I. and Chevalier, Y., 1977, Proc. Photovoltaic Solar Energy Conf., Luxembourg, p. 967, "Silicon Double Solar Cell."

Chappell, T.I., 1979, *IEEE Trans. Electron Devices ED-26,* 1091, "The V-groove Multijunction Solar Cell."

Chappell, T.I., 1980, *IEEE Trans. Electron Devices ED-27,* 760, "A Study of the Conversion Efficiency Limit of p^+-i-n^+ Silicon Solar Cells in Concentrated Sunlight."

Chen, P.J., Pao, S.C., Neugroschel, A., and Lindholm, F.A., 1978, *IEEE Trans. Electron Devices ED-25,* 386, "Experimental Determination of Series Resistance of p-n Junction Diodes and Solar Cells."

Chiang, S.Y., Carbajal, B.G., and Wakefield, G.F., 1978, *IEEE Trans. Electron Devices ED-25,* 1405, "Improved Performance Thin Solar Cells."

Chin, D.J. and Navon, D.H., 1980, *Solid-State Electron.* (to be published), "Two-Dimensional Analysis of the Interdigitated Back Contact Solar Cell."

Deal, B.E., Sklar, M., Grove, A.S., and Snow, E.H., 1967, *J. Electrochem. Soc. 114,* 266, "Characteristics of the Surface-State Charge (Q_{SS}) of Thermally Oxidized Silicon."

de Graaff, H.C., Slotboom, J.W., and Schmitz, A., 1977, *Solid-State Electron 20,* 515, "The Emitter Efficiency of Bipolar Transistors."

de Graaff, H.C. and Slotboom, J.W., 1976, *Solid-State Electron. 19,* 809, "Some Aspects of LEC Transistor Behavior."

Dunbar, P.M. and Hauser, J.R., 1977, *Solid-State Electron. 20,* 697, "Theoretical Effects of Surface Diffused Region Lifetime Models on Silicon Solar Cells."

Duncan, C.S., Seidensticker, R.G., McHugh, J.P., Hopkins, R.H., Skutch, M.E., Driggers, J.M., and Hill, F.E., 1980, Proc. 14th IEEE Photovoltaic Specialists Conf., p. 25, "Development of Processes for the Production of Low Cost Silicon Dendritic Web for Solar Cells."

Dziewior, J. and Schmid, W., 1977, *Appl. Phys. Lett. 31,* 346, "Auger Coefficients for Highly Doped and Highly Excited Silicon."

Ehrenrich, H. et al., 1979, Principal Conclusions of the APS Study Group on Solar Photovoltaic Energy Conversions, published by the American Physical Society.

ERDA, 1977, "Terrestrial Photovoltaics Measurement Procedures," ERDA/NASA/1022-77/16.

Fistul', V.I., 1969, *Heavily Doped Semiconductors,* Plenum Press, New York.

Fossum, J.G., 1976, *Solid-State Electron. 19,* 269, "Computer-Aided Numerical Analysis of Silicon Solar Cells."

Fossum, J.G., Burgess, E.L., and Lindholm, F.A., 1978, *Solid-State Electron. 21,* 729, "Silicon Solar Cell Designs Based on Physical Behavior in Concentrated Sunlight."

Fossum, J.G., Lindholm, F.A., and Shibib, M.A., 1979, *IEEE Trans. Electron Devices, ED-26,* 1294, "The Importance of Surface Recombination and Energy-Gap Narrowing in p-n Junction Silicon Solar Cells."

Fossum, J.G., Nasby, R.D., and Pao, S.C., 1980, *IEEE Trans. Electron Devices, ED-27,* 785, "Physics Underlying the Performance of Back-Surface-Field Solar Cells."

Frank, R.I., Goodrich, J.L., and Kaplow, R., 1980, Proc. 14th IEEE Photovoltaic Specialists Conf., p. 423, "A Low Series Resistance Silicon Photovoltaic Cell for High Intensity Applications."

Godfrey, R.B. and Green, M.A., 1979, *Appl. Phys. Lett. 34,* 860, "High-Temperature Lifetesting of Al/SiO_x/p-Si Contacts for MIS Solar Cells."

Godfrey, R.B. and Green, M.A., 1980, *IEEE Trans. Electron Devices ED-27,* 737, "High-Efficiency Silicon minMIS Solar Cells — Design and Experimental Results."

Goradia, C. and Goradia, M.G., 1976, Proc. 12th IEEE Photovoltaic Specialists Conf., p. 789, "Recent Experimental Results on High Intensity (HI) Edge-Illuminated Multijunction Silicon Solar Cells."

Goradia, C. and Sater, B.L., 1977, *IEEE Trans. Electron Devices ED-24,* 342, "A First Order Theory of the p^+-n-n^+ Edge-Illuminated Silicon Solar Cell at Very High Injection Levels."

Graff, K. and Fischer, H., 1979, *Top. Appl. Phys. 31,* p. 173, "Carrier Lifetime in Silicon and Its Impact on Solar Cell Characteristics."

Green, M.A., 1977, *Solid-State Electron. 20,* 265, "General Solar Cell Curve Factors Including the Effects of Ideality Factor, Temperature, and Series Resistance."

Hall, R.N. and Soltys, T.J., 1980, Proc. 14th Photovoltaic Specialists Conf., p. 550, "Polka Dot Solar Cell."

Hauser, J.R. and Dunbar, P.M. 1977, *IEEE Trans. Electron Devices ED-24,* 305, "Performance Limitations of Solar Cells."

Heasell, E.L., 1980, *Solid-State Electron. 23,* 183, "On the Role of Degeneracy in the 'Heavy-Doping' Phenomenon."

Henry, C.H., Logan, R.A., and Merritt, F.R., 1978, *J. Appl. Phys. 49,* 3530, "The Effect of Sur-

face Recombination on Current in $Al_xGa_{1-x}As$ Heterojunctions."

Herlet, 1968, *Solid-State Electron. 11,* 717, "The Forward Characteristics of Silicon Power Rectifiers at High Current Densities."

Hovel, H.J., 1973, Proc. 10th Photovoltaic Specialists Conf., p. 34, "Effect of Depletion Layer Recombination Currents on the Efficiencies of Si and GaAs Solar Cells."

Hovel, H.J., 1975, *Semiconductor and Semimetals, 11,* "Solar Cells," Academic Press, New York.

Hu, C. and Drowley, C., 1978, Proc. 13th IEEE Photovoltaic Specialists Conf., p. 786, "Open Circuit Voltage of High Intensity Silicon Solar Cells."

Iles, P.A., 1977, *J. Vac. Sci. Technol. 14,* 1100, "Antireflection Coatings for Solar Cells."

Iles, P.A. and Soclof, S.I., 1975, Proc. 11th Photovoltaic Specialists Conf., p. 19, "Effect of Impurity Doping Concentration on Solar Cell Output."

Johnston, W.D., Jr., 1980, "Solar Voltaic Cells," Marcel Dekker.

Kalejs, J.P., Mackintosh, B.H., Sachs, E.M., and Wald, F.V., 1980, Proc. 14th IEEE Photovoltaic Specialists Conf., p. 13, "Progress in the Growth of Wide Silicon Ribbons by the EFG Technique at High Speed Using Multiple Growth Stations."

Kendall, D., 1969, "Conference on the Physics and Application of Lithium Diffused Silicon," NASA (unpublished).

Kern, W. and Tracy, E., 1980, *RCA Rev. 41,* 133, "Titanium Dioxide Antireflection Coating for Silicon Solar Cells by Spray Deposition."

Keyes, R.W., 1976, *Comments Solid State Phys. 7,* 149, "The Energy Gap of Impure Silicon."

Kleta, J.K. and Pulfrey, D.L., 1980, *IEEE Electron Device Lett. EDL-1,* 107, "On the Stability of MIS Solar Cells."

Lammert, M.D. and Schwartz, R.J., 1977, *IEEE Trans. Electron Devices ED-24*, 337, "The Interdigitated Back Contact Solar Cell: A Silicon Solar Cell for Use in Concentrated Sunlight."

Landsberg, P.T., 1980, "Semiconductor Statistics," Chapter 8 in *Handbook on Semiconductors,* W. Paul, ed., North Holland Publishing Co.

Lauwers, P., Van Meerbergen, J., Bulteel, P., Mertens, R., and Van Overstraeten, R., 1978, *Solid-State Electron. 21*, 747, "Influence of Bandgap Narrowing on the Performance of Silicon n-p Solar Cells."

Lee, K. and Nussbaum, A., 1980, *Solid-State Electron. 23*, 655, "The Influences of Traps on the Generation-Recombination Current in Silicon Diodes."

Li, S.S., 1978, *Solid-State Electron. 21*, 1109, "The Dopant Density and Temperature Dependence of Hole Mobility and Resistivity in Boron Doped Silicon."

Li, S.S. and Thurber, W.R., 1977, *Solid-State Electron. 20*, 609, "The Dopant Density and Temperature Dependence of Electron Mobility and Resistivity in n-Type Silicon."

Lindholm, F.A. and Fossum, J.G., 1980, Proc. 14th Photovoltaic Specialists Conf., p. 680, "Physics Underlying Recent Improvements in Silicon Solar-Cell Performance."

Lindholm, F.A., Fossum, J.G., and Burgess, E.L., 1979, *IEEE Trans. Electron Devices ED-26*, 165, "Application of the Superposition Principle to Solar-Cell Analysis."

Lindmayer, J. and Allison, J.F., 1976, U.S. Patent 3,982,964, "Dotted Contact Fine Geometry Solar Cell."

Lochmann, W., 1978, *Phys. Status Solidi (a) 45* 423, "Phonon-Assisted Auger Recombination in Indirect Gap Semiconductors."

Mahan, G.D., 1980, *J. Appl. Phys. 51*, 2634, "Energy Gap in Si and Ge: Impurity Dependence."

Marshak, A.H. and Shrivastava, 1979, *Solid-State Electron. 22*, 567, "Law of the Junction for Degenerate Material with Position-Dependent Band Gap and Electron Affinity."

Meulenberg, A., 1977, *J. Energy 1*, 151, "The Sawtooth Coverslide: A New Means of Coupling Light into Solar Cells."

Meulenberg, A., Allison, J.R., and Arndt, R.A., 1980, Proc. 14th Photovoltaic Specialists Conf., San Diego, p. 161, "Thin n-i-p Silicon Solar Cell."

Neugroschel, A., 1980, *IEEE Trans. Electron Devices ED-27*, 287, "MOS and Oxide-Charge-Induced (OCI) BSF Solar Cells."

Neugroschel, A., Lindholm, F.A., and Pao, S.C., 1978, *Appl. Phys. Lett. 33*, 168, "Emitter Current Suppression in a High-Low-Junction Emitter Solar Cell Using an Oxide-Charge-Induced Electron Accumulation Layer."

Ng, K.K. and Card, H.C., 1980, *IEEE Trans. Electron Devices ED-27*, 716, "A Comparison of Majority- and Minority-Carrier Silicon MIS Solar Cells."

Possin, G.E., Adler, M.S., and Baliga, B.J., 1980, *IEEE Trans. Electron Devices ED-27*, 983, "Measurement of Heavy Doping Parameters in Silicon by Electron Beam Induced Current."

Queisser, H.J., 1962, *Solid-State Electron. 5*, 1, "Forward Characteristics and Efficiencies of Silicon Solar Cells."

Rasch, K.D., Roy, K., Schilling, R., and Fischer, H., 1980, Proc. 14th Photovoltaic Specialists Conf., p. 141, "Compatibility of BSR and BSF Solar Cell Technology."

Redfield, D., 1975, *Adv. Phys. 24*, 463, "Transport Properties of Electrons in Energy Band Tails."

Redfield, D., 1980, *IEEE Trans. Electron Devices ED-27*, 766, "Unified Model of Fundamental Limitations on the Performance of Silicon Solar Cells."

Restrepo, F. and Backus, C.E., 1976, *IEEE Trans. Electron Devices ED-23*, 1195, "On Black Solar Cells and the Tetrahedral Texturing of Silicon Surfaces."

Revesz, A.G., Allison, J.F., and Reynolds, J.H., 1976, *COMSAT Tech. Rev. 6*, 57, "Tantalum

Oxide and Niobium Oxide Films in Silicon Solar Cells."

Ruppel, W. and Wurfel, P., 1980, *IEEE Trans. Electron Devices ED-27*, 877, "Upper Limit for the Conversion of Solar Energy."

Sah, C.T., 1962, *IEEE Trans. Electron Devices ED-9*, 94, "Effect of Surface Recombination and Channel on P-N Junction and Transistor Characteristics."

Sah, C.T., 1978, Contract Report Prepared under Consultant Agreement 660411 with Jet Propulsion Laboratory, unpublished.

Sah, C.T., Lindholm, F.A., and Fossum, J.G., 1978, *IEEE Trans. Electron Devices ED-25*, 66, "A High-Low Junction Emitter Structure for Improving Silicon Solar Cell Efficiency."

Sah, C.T., Noyce, R.N., and Shockley, W., 1957, *Proc. IRE 45*, 1228, "Carrier Generation and Recombination in P-N Junctions and P-N Junction Characteristics."

Schlangenotto, H. and Maeder, H., 1979, *IEEE Trans. Electron Devices ED-26*, 191, "Spatial Composition and Injection Dependence of Recombination in Silicon Power Device Structures."

Schlangenotto, H., Maeder, H., and Gerlach, W., 1974, *Phys. Status Solidi (a) 21*, 357, "Temperature Dependence of the Radiative Recombination Coefficient in Silicon."

Schuster, K., 1965, *Solid-State Electron. 8*, 427, "Determination of the Lifetime from the Stored Carrier Charge in Diffused psn Rectifiers."

Shewchun, J., Burk, D., and Spitzer, M.B., 1980, *IEEE Trans. Electron Devices ED-27*, 705, "MIS and SIS Solar Cells."

Shibib, M.A., Lindholm, F.A., and Therez, F., 1979, *IEEE Trans. Electron Devices ED-26*, 959, "Heavily Doped Transparent-Emitter Regions in Junction Solar Cells, Diodes, and Transistors."

Shockley, W. and Queisser, H.J., 1961, *J. Appl. Phys. 32*, 510, "Detailed Balance Limit of Efficiency of p-n Junction Solar Cells."

Sinha, A. and Chattopadhyaya, S.K., 1979, *Solid-State Electron. 22*, 849, "Temperature Dependence of Open-Circuit Photovoltage of a Back-Surface Field Semiconductor Junction."

Slotboom, J.W., 1977, *Solid-State Electron. 20*, 279, "The pn-Product in Silicon."

Spenke, E., 1968, *Solid-State Electron. 11*, 1119, "Notes on the Theory of the Forward Characteristic of Power Rectifiers."

Stirn, R.J., 1972, Proc. 9th Photovoltaic Specialists Conf., p. 72, "Junction Characteristics of Silicon Solar Cells."

Svantesson, K.G. and Nilsson, N.G., 1979, *J. Phys. C 12*, 5111, "The Temperature Dependence of the Auger Recombination Coefficient of Undoped Silicon."

Sze, S.M., 1969, *Principles of Semiconductor Devices*, John Wiley and Sons, New York, (new edition to be published in 1981).

Tang, D.D., 1980, *IEEE Trans. Electron Devices ED-27*, 563, "Heavy Doping Effects in p-n-p Bipolar Transistors."

Tarr, N.G. and Pulfrey, D.L., 1980, *IEEE Trans. Electron Devices ED-27*, 771, "The Superposition Principle for Homojunction Solar Cells."

Tarr, N.G., Pulfrey, D.L., and Iles, P.A., 1980, *J. Appl. Phys. 51*, 3926, "An Induced Back Surface Field Solar Cell Employing a Negative Barrier Metal-Insulator-Semiconductor Contact."

Theriault, R.E. and Thomas, R.E., 1978, *Int. Electron Devices Meeting Tech. Dig.*, p. 85, "A Low-Temperature CVD Oxide Process of Inversion Layer MIS Solar Cells."

Thomas, R.E., North, R.B., and Norman, C.E., 1980, *IEEE Electron Device Lett. EDL-1*, 79, "Low Cost — High Efficiency MIS/Inversion Layer Solar Cells."

Tsuya, N. et al., 1980, *Jpn. J. Appl. Phys. 19, Suppl. 19-1*, 655, "Polycrystalline Silicon Ribbons Made by Rapid Quenching Methods."

Van Meerbergen, J., Nijs, J., Mertens, and R. Van Overstraeten, R., 1978, Proc. 13th Photovoltaic Specialists Conf., p. 66, "Measurement of Bandgap Narrowing and Diffusion Length in Heavily Doped Silicon."

Varshni, Y.P., 1967, *Physica 34*, 149, "Temperature Dependence of the Energy Gap in Semiconductors."

Weakliem, H.A. and Redfield, D., 1979, *J. Appl. Phys. 50*, 1491, "Temperature Dependence of the Optical Properties of Silicon."

Weaver, H.T. and Nasby, R.D., 1980, to be published, "Analysis of High-Efficiency Solar Cells."

Wohlgemuth, J. and Scheinine, A., 1980, Proc. 14th IEEE Photovoltaic Specialists Conf., p. 151, "New Developments in Vertical Junction Silicon Solar Cells."

Wolf, H.F., 1971, *Semiconductors*, John Wiley and Sons, Inc., New York.

Wolf, M., 1980, *IEEE Trans. Electron Devices ED-27*, 751, "Updating the Limit Efficiency of Silicon Solar Cells."

Wolf, M., Noel, G.T., and Stirn, R.J., 1977, *IEEE Trans. Electron Devices ED-24*, 419, "Investigation of the Double Exponential in the Current-Voltage Characteristics of Silicon Solar Cells."

Wolf, M. and Rauschenbach, H., 1963, *Adv. Energy Conversion 3*, 455, "Series Resistance Effects on Solar Cell Measurements."

Yaws, C.L., Li, K.-Y., Fang, C.S., Lutwack, R., Hsu, G., and Leven, H., 1980, *Sol. Energy 24*, 359, "New Technologies for Solar Energy Silicon: Cost Analysis of BCL Process."

H80CRD274
CAMPBELL VC 6065102090
GENERAL ELECTRIC CO.
TB DEPT 6-183 EP
SYRACUSE NY 13221

R.N. Hall

SILICON PHOTOVOLTAIC CELLS

Report No. 80CRD274
January 1981

GENERAL ELECTRIC COMPANY
CORPORATE RESEARCH AND DEVELOPMENT
P.O. BOX 8, SCHENECTADY, N.Y. 12301